Volume 54
Number 44
28 November 2025
Pages 16257-16630

Dalton Transactions

An international journal of inorganic chemistry

rsc.li/dalton

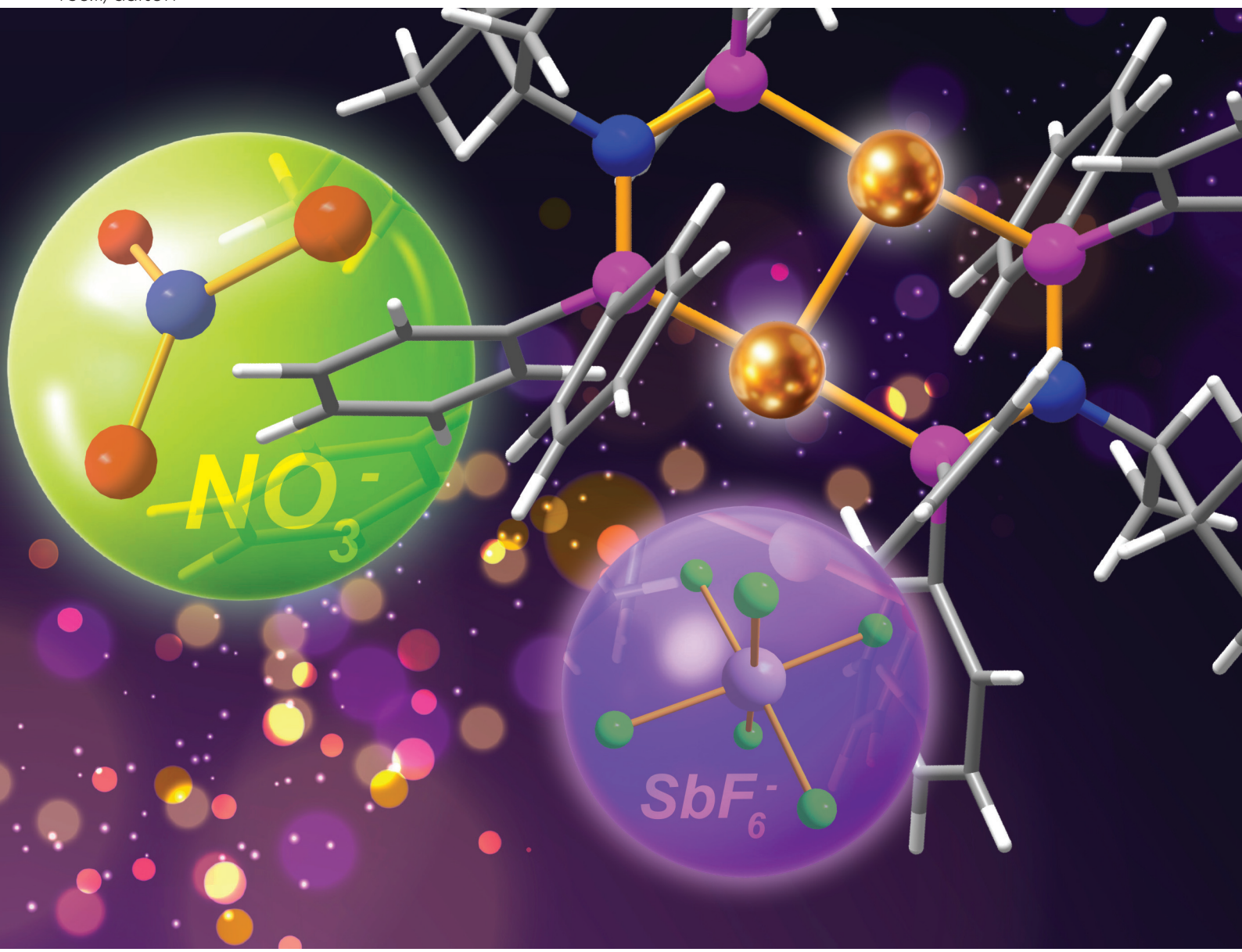

ISSN 1477-9226

ROYAL SOCIETY OF CHEMISTRY

PAPER

Hendrik G. Visser *et al.*

Ligand and counter-ion effects on the photoluminescence of dinuclear bis(diphenylphosphino)amine gold(I) complexes

Dalton Transactions

ROYAL SOCIETY OF CHEMISTRY

PAPER

View Article Online
View Journal | View Issue

Cite this: *Dalton Trans.*, 2025, **54**, 16393

Ligand and counter-ion effects on the photoluminescence of dinuclear bis(diphenylphosphino)amine gold(I) complexes

Christo van Staden, [a] Robin E. Kroon, [b] Cameron Matthews,[a] Lyudmila V. Moskaleva, [a] Kgalaletso P. Otukile,[a] Dumisani V. Kama,[a] Marietjie Schutte-Smith [a] and Hendrik G. Visser *[a]

We report the synthesis and characterization of two series of dinuclear gold(I) complexes with different *N*-substituted (R) bridging bis(diphenylphosphino)amine (PNP) ligands (R = *n*-butyl, cyclobutyl, cyclopentyl, cyclohexyl, 2-butyl, 1,2-dimethylpropyl): paired with either nitrate or hexafluoroantimonate counter-ions. Single-crystal X-ray diffraction studies on four hexafluoroantimonate salts revealed Au···Au distances ranging from 2.754 Å to 2.830 Å. These crystal structures provide the first crystallographic evidence of an aliphatic *N*-substituent in complexes of this nature. Despite these structural variations, solid-state photoluminescence studies showed no significant variation in the emission and excitation wavelengths of these complexes across the *N*-substituted series. In contrast, significant differences in the photophysical properties (especially the emission energies and lifetimes) were observed as a function of the counterion, highlighting the important role of anion identity in modulating photophysical properties. Time-dependent density functional theory (TD-DFT) computations at the TPSSh level reproduced the experimental trends and attributed the counterion-induced emission redshift to weak bonding interactions between the gold centers and coordinating anions, such as nitrate and chloride.

Received 10th September 2025,
Accepted 21st October 2025

DOI: 10.1039/d5dt02181b

rsc.li/dalton

Introduction

Gold(I) complexes have attracted significant attention due to their intriguing photophysical properties, notably their strong luminescence in the solid state.[1–5] These properties have enabled applications in sensing, optoelectronics, and materials chemistry. For example, a combination of yellow light-emitting gold nanoclusters with blue light-emitting poly(*N*-vinyl carbazole) as a host resulted in a white light-emitting LED source.[6,7] Other applications based on the strong luminescence of gold include its use as a chemosensor to detect the presence of other metals or pollutants in water.[8,9] In particular, dinuclear and polynuclear Au(I) complexes often exhibit pronounced luminescence due to aurophilic interactions – non-covalent attractions between closed-shell Au(I) centers – that are highly sensitive to structural and environmental factors.[10,11]

Aurophilic interactions, typically characterized by Au···Au distances in the range of 2.5–3.5 Å, arise from relativistic effects and dispersion interactions, leading to electronic configurations conducive to emissive excited states.[12–16] Their strength and prevalence distinguish gold from its coinage counterparts, Ag(I) and Cu(I), and offer a structural handle for tuning luminescence.

Aurophilic interactions can be either unsupported, semi-supported or fully supported by bridging ligands, as shown in Fig. 1.[17]

Several computational studies of complexes with aurophilic interactions predicted a significant decrease in the Au···Au distance from the singlet ground states with respect to the corresponding emitting triplet excited states, which was attributed to the formation of an Au–Au covalent bond in the excited state,

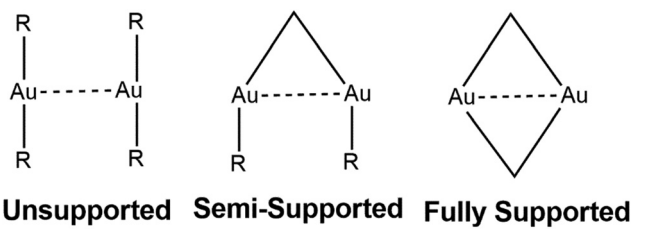

Fig. 1 Visual representation of unsupported, semi-supported, and fully supported aurophilic interactions.

[a]*Department of Chemistry, University of the Free State, PO Box 339, Bloemfontein 9300, South Africa. E-mail: visserhg@ufs.ac.za*
[b]*Department of Physics, University of the Free State, PO Box 339, Bloemfontein 9300, South Africa*

consistent with the formulation of the electronic transition that involves promotion of an electron from an Au–Au (d,s)σ* antibonding to a (p,s)σ bonding orbital.[18–24] However, computational studies of the excited states of such complexes are quite rare due to the complexity and high computational cost of excited state calculations compared to ground state calculations.

Photophysical properties of aurophilic complexes are not governed solely by metal–metal distances; other factors such as ligands, crystal packing, solvation, and – importantly – counterions also play a critical role in determining emission wavelengths and lifetimes.[24–27,30] Mononuclear gold complexes can also exhibit aurophilic interactions, forming so-called excimers/exciplexes.[4,28–30] These are complexes that are formed by interatomic/intermolecular bonding only in the excited state.[20,22,31,32] The formation of exciplexes with solvent molecules has also been observed in several studies involving gold(I) dimers.[18,19,33–35] Other examples show that solvent molecules can disrupt the Au···Au interaction and have a quenching effect on the luminescence.[36]

Despite the widespread focus on ligand modifications and aurophilic geometry,[28,37–39] the impact of counterions on emission properties remains underexplored. Counterions can modulate excited-state dynamics through ion-pairing, structural rearrangement, or interference with aurophilic interactions.[40–42] Prior studies suggest that weakly coordinating anions may alter the crystal structures and luminescent properties of compounds with aurophilic interactions,[42] whereas more coordinating anions may quench luminescence or induce spectral shifts.[40] Yet, systematic investigations isolating the effect of the counterion, while keeping the metal core and ligand environment constant, are limited.

In this study, we present a family of fully supported bis(μ_2-PNP)-digold(I) complexes [PNP = *N*-substituted bis(diphenylphosphino)amine ligands] featuring aliphatic *N*-substituents (R = *n*-butyl, cyclobutyl, cyclopentyl, cyclohexyl, and 2-butyl). While studies of similar complexes with aromatic *N*-substituents were previously reported,[43,44] no *N*-alkyl substituted bis(diphenylphosphino)amine Au(I)–Au(I) complexes have ever been described crystallographically. Crystallographic analyses reveal variations in the Au···Au distances across the series (2.754–2.830 Å). However, spectroscopic studies show that these structural differences do not result in significant changes in the excitation and emission maxima. In contrast, significant shifts in emission wavelength and luminescence lifetime are observed upon varying the counterion (Cl^-, NO_3^-, SbF_6^-), indicating that anion identity plays an important role in dictating the photophysical response.

Time-dependent density functional theory (TD-DFT) calculations on selected complexes support the experimental findings by correlating counterion-dependent changes in the excited-state electronic structure with the observed photophysical trends. By isolating the influence of counterions within a consistent ligand framework, this work contributes to a more nuanced understanding of structure–property relationships in luminescent Au(I) systems.

Results and discussion

Synthesis

Six PNP ligands (**L1–L6**) were successfully synthesized (Fig. 2). The corresponding bis(μ_2-(PNP))-di-gold(I) complexes with nitrate counterions (**1a–6a**) were obtained as illustrated in Fig. 3. Reaction of these ligands with [AuCl(Me_2S)] afforded mixtures of monomeric and dimeric chloride precursors, as previously reported.[43,44] Upon treatment with $AgNO_3$, both precursors were converted cleanly into the corresponding nitrate salts, $Au_2\{\mu_2\text{-(PNP)}\}_2(NO_3)_2$ (**1a–6a**) Without the need to isolate the intermediates. However, the dimeric chlorido intermediate, dichloridobis(μ_2-bis(diphenylphosphino)-*n*-butylamine)-di-gold(I) (**1c**), was successfully isolated by crystallization.

The structures of the complexes were confirmed by multinuclear NMR, IR, and UV/Vis spectroscopy. In particular, the formation of the dimeric gold(I) complexes is evidenced by the ^{31}P NMR spectra which consistently display a single resonance at ~95 ppm (ref. 43 and 44) (see S2: SI). The purity of the products was also verified by elemental analysis.

The corresponding hexafluoroantimonate complexes, $Au_2\{\mu_2\text{-(PNP)}\}_2(SbF_6)_2$ (**1b–6b**), were initially synthesized through a counterion substitution by adding an excess of silver hexafluoroantimonate to nitrates **1a–6a**. In order to obtain better yields and cleaner products, a similar procedure to the synthesis of **1a–6a**, with intermediate chlorido precursors, was used to synthesize complexes **1b–6b** (Fig. 3). These complexes were likewise characterized by multinuclear NMR, and UV/Vis spectroscopy, and elemental analysis.

X-ray crystallography

The crystal structures of **1b**, **2b**, **4b** and **5b** were obtained and are illustrated in Fig. 4. The X-ray structural data can be found in S1: Supplementary SC-XRD Information. The complexes showed residual densities around the gold atoms. While such features can sometimes arise from limitations in data quality, they are also commonly observed for heavier atoms and are often attributed to Fourier transformed ripple effects resulting from the scattering nature of the gold atoms.

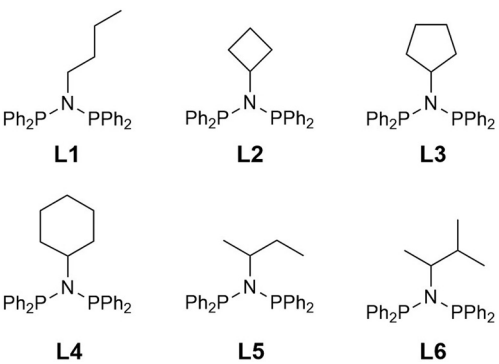

Fig. 2 Graphical depiction of the six bis(diphenylphosphino)amine (PNP) ligands (**L1–L6**) utilized in this study.

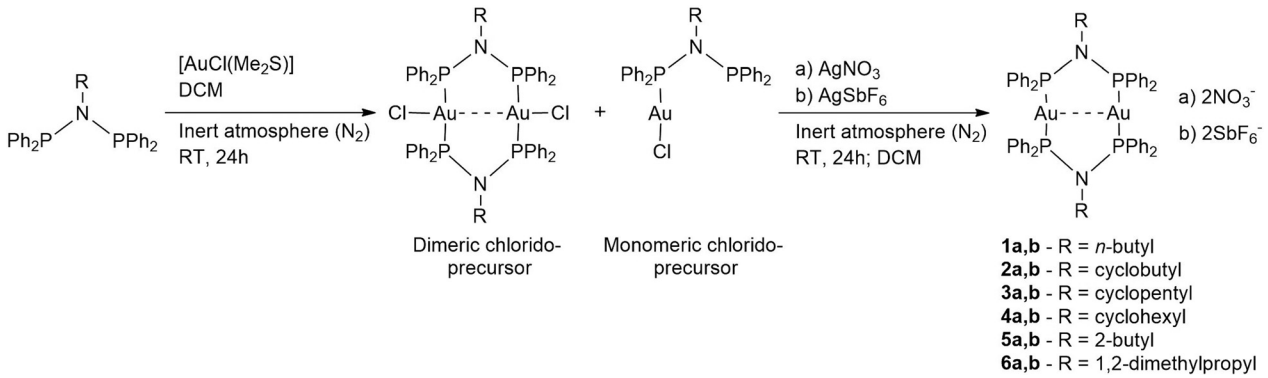

Fig. 3 Schematic representation of the synthetic procedure of the Au(I) complexes **1a–6a** and **1b–6b**.

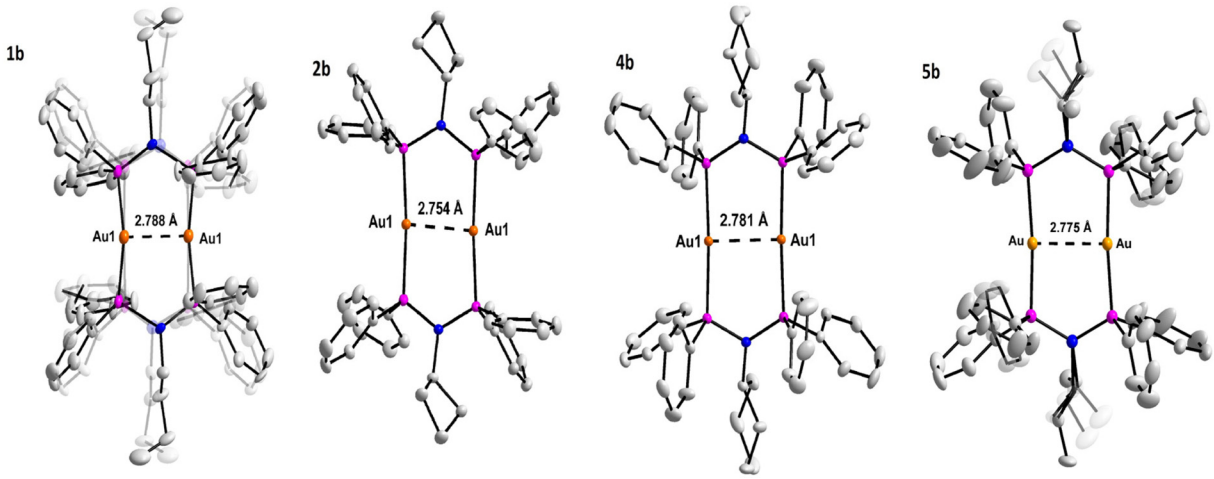

Fig. 4 The atomic structures of **1b**, **2b**, **4b**, **5b**. Hydrogen atoms and all labels except for gold are omitted for clarity. Ellipsoids are drawn at 50% probability. Counterions are omitted for clarity. Gray = C, pink = P, blue = N.

1b, **2b**, **4b** and **5b** all crystallized in the monoclinic space group $P2_1/n$, with half of the dimeric molecule present in the asymmetric unit and the second half generated by the $(1 - x, 1 - y, 1 - z)$ symmetry operation. Except for the gold atoms and hexafluoroantimonate counterions, the entire structure of **1b** is positionally disordered. In **5b**, the *N*-substituent on the PNP ligand (the 2-butyl group) and one of the phenyl rings are positionally disordered.

The base structures of complexes **1b**, **2b**, **4b**, **5b** are all identical, apart from the *N*-substituents on the two bridging PNP ligands. These ligands are coordinated to two Au(I) atoms, forming a cyclic complex with two hexafluoroantimonate counterions. The complexes showed different types of weak inter- and intramolecular interactions, which are described in detail in the SI (see S1: Supplementary SC-XRD Information). Table 1 contains selected bond lengths and angles of **1b**, **2b**, **4b**, **5b** for comparison.

The data presented in Table 1 illustrate the subtle geometric variations associated with the different *N*-substituents. In the disordered regions of **1b** and **5b**, the two N–C distances differ by 0.09 Å and 0.06 Å, respectively, and the P1–Au–P2 angle in **1b** varies by about 10° between the two disordered components. Overall, however, the P1–Au–P2 and P–N–P angles, as well as the N–C and Au–P distances, are consistent across all four structures. The Au···Au distances vary by up to ~0.04 Å, with all values lying within the 2.7–2.8 Å range, thus confirming the presence of aurophilic interactions.

Table 1 Crystal data and structure refinement data for **1b**, **2b**, **4b**, **5b**

	Bond lengths [Å] and bond angles [°]			
Bonds and angles	**1b**	**2b**	**4b**	**5b**
Au···Au	2.7884(6)	2.7537(3)	2.7812(3)	2.7752(3)
Au–P1	2.2490(7) 2.3710(7)	2.3082(6)	2.3087(6)	2.3044(7)
Au–P2	2.2590(6) 2.3510(6)	2.3042(6)	2.3229(6)	2.3199(7)
N–C	1.501(1) 1.592(2)	1.510(3)	1.5240(2)	1.56(1) 1.51(2)
P–N–P	120.7(6) 118.0(7)	120.3(1)	117.0(9)	118.5(1)
P1–Au–P2	150.4(2) 160.3(2)	170.9(2)	170.4(2)	168.2(2)

The packing of complexes **1b** and **2b** differs from that of **4b** and **5b**. In **1b** and **2b**, the molecules adopt a head-to-tail arrangement that propagates semi-diagonally along the *a*-axis when viewed along the *b*-axis. By contrast, **4b** and **5b** exhibit a head-to-tail packing along the *c*-axis, also evident when viewing the complex along the *b*-axis. In all four structures, the SbF_6^- counterion occupies a constant position, located between the gold atoms of complexes stacked above and below each other when viewed along the *b*-axis.

Photophysical studies

Di- and polynuclear gold(I) complexes have been the subject of intense research due to their intriguing luminescence properties.[45,46] These complexes often exhibit interesting and rich photophysical properties influenced by aurophilic interactions on the electronic structure. Particularly intriguing is the relationship between the observed emission and the presence of Au···Au short contacts.[37,38] The choice of ligands may influence the photoluminescence characteristics of these complexes. By altering the energy levels within the complexes, ligands can affect both the absorption and emission wavelengths.[47,48] Despite considerable research efforts, the relationship between the structure and emission energy of luminescent gold(I) complexes remains elusive. Several reports in literature have attempted to correlate crystallographic Au···Au distances with emission energies, but this task remains challenging due to the diverse complexity of these systems.[28,37–39]

We have investigated the photophysical properties of dinuclear gold(I) bis(diphenylphosphino)amine complexes, aiming to explore the effect of different *N*-substituents and counterions on the absorption and emission profiles. The excitation and emission spectra of the synthesized dinuclear gold(I) complexes **1a–6a** (with NO_3^- counterions) and **1b–6b** (with SbF_6^- counterions) were obtained in the solid-state and are shown in Fig. 5. The summarized data in Table 2 shows similar results for different *N*-substituents, which indicates that the ligands have limited impact on the photoluminescence. However, the influence of the counterion was significant and resulted in an emission shift from green light (540 nm–552 nm) for complexes **1a–6a** with NO_3^- counterions to blue light (430 nm–435 nm) for complexes **1b–6b** with SbF_6^- counterions. The complexes **1b–6b** also tended to feature two excitation peaks, located to either side of the single excitation wavelength found for the complexes **1a–6a**.

Photophysical studies of complexes similar to those studied in this work, namely bis(μ_2-bis(diphenylphosphino)-2,6-isopropylphenylamine)-di-gold(I) bis(hexafluoroantimonate) and bis(μ_2-bis(diphenylphosphino)-aniline)-di-gold(I) bis(hexafluoroantimonate), that differ only in the *N*-substituents on the PNP backbone, have been reported previously.[43] The quantum yields for these complexes were reported to be 59% and 37%, respectively, higher than the values obtained here (maximum 29% for complex **1b**). The average excitation and emission wavelengths of the complexes with the hexafluoroantimonate counterion measured in the present work (364 nm for excitation and 432 nm for emission) were somewhat higher than the values reported in the aforementioned study (average 322 nm for excitation and 423 nm for emission). The difference could be attributed to the different electronic properties of the aromatic substituents on the N atom of the PNP ligands (R = Ph, and 2,6-diisopropylphenyl) used in the previous work[43] compared to the aliphatic R groups of complexes **1a–6a**. Aromatic R groups are less electron donating than the aliphatic ones,[48] therefore, it is expected that they should result in a blue-shift of the emission wavelength, which is consistent with the comparison between our measurements and those of the previous work[43] for both absorption and emission. Similar to the emission data, the lifetimes differ significantly with the change in counterion, being 2.00–2.45 μs for the **a** group and 0.18–1.26 μs for the **b** group. The lifetimes found in our study are somewhat longer than those reported in the previous study of similar complexes with an aromatic R group.[43] (0.20 μs and 0.05 μs for the two complexes, respectively).[43] Neither the quantum yield nor the lifetimes showed a clear systematic change with the variation of the steric bulk of the *N*-substituent on the PNP ligand.

Computational studies of luminescence

To understand the origin of the observed photophysical properties of the studied family of complexes, we performed TD-DFT calculations for two representative complexes, with R = "Bu", *i.e.* *n*-butyl (considering NO_3^- counterions, *i.e.* sample **1a**, SbF_6^- counterions, *i.e.* sample **1b**, and also Cl^- counterions, sample **1c**) as well as R = "2,6Me", *i.e.* 2,6-dimethylphenyl (with SbF_6^- counterions) for which experimental photophysical data is available for comparison in the literature.[43]

There are a number of calculations in the literature that elucidate the molecular orbitals (MOs) of eight-membered dinuclear Au(I) complexes with bridging ligands, such as phosphines, N-heterocyclic carbenes, and dichalcogenophosphinates.[18,19,21–23,49,50] In the early study by Fackler's group, the MOs responsible for the absorption and emission in the model $[Au_2(H_2PCH_2PH_2)_2]^{2+}$ complex were described in terms of the Au atomic orbitals: $d\sigma^* \rightarrow p\sigma$ (main absorption band).[49] Here, the $d\sigma^*$ refers to the antibonding combination of the Au $5d_{z^2}$ orbitals and $p\sigma$ refers to the bonding combination of the Au $6p_z$ orbitals. Subsequently, these or similar notations have been frequently used in literature on the luminescence of dinuclear gold-phosphine complexes. In the following paragraphs, we will also use this notation, although the orbitals denoted, especially the lowest occupied molecular orbital (LUMO) denoted $p\sigma$, are not purely metallic in nature.

The frontier MOs for the ground state of complexes **1a**, **1b**, and **1c** are shown in Fig. 6–8. The qualitative nature and ordering of the frontier MOs are similar for the two *N*-substituents considered (R = Bu and 2,6Me) and are not altered by the choice of a density functional, TPSSh or B3LYP, but the type of counterions change the ordering of the top occupied MOs. For **1b** (with weakly coordinating SbF_6^- anions), the highest occupied molecular orbital (HOMO) is largely metal-centered and

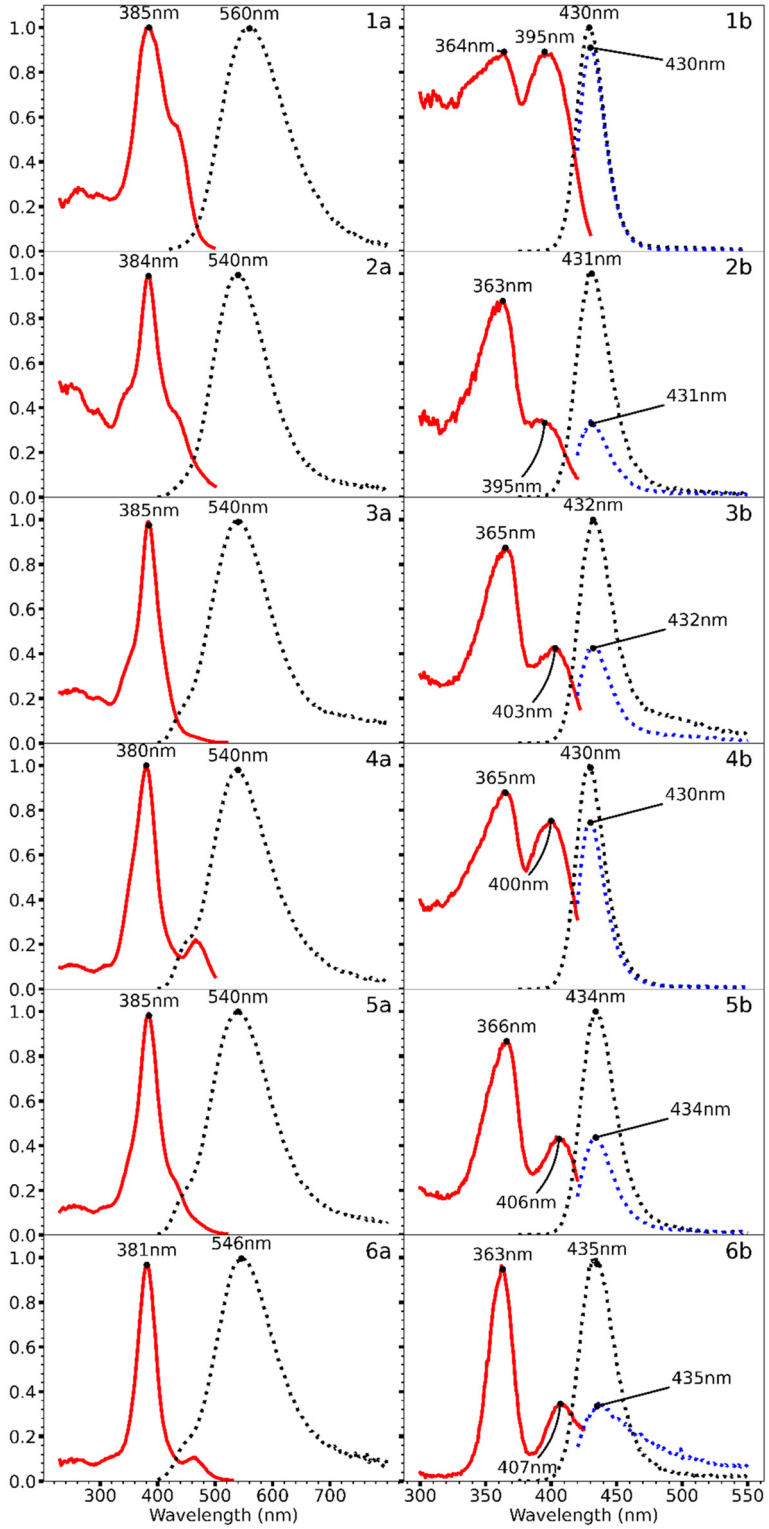

Fig. 5 The excitation and emission spectra of **1a–6a** (NO_3^- counterions) and **1b–6b** (SbF_6^- counterions) in the solid-state. Excitation spectra are shown as red solid lines, while emission spectra are shown as grey dotted lines.

includes contributions from Au 6s and 5d orbitals in an antibonding σ* combination. In contrast to the prototypical $[Au_2(H_2PCH_2PH_2)_2]^{2+}$ complex,[49] for the complexes of this study, the short Au···Au contacts lead to a greater involvement of the Au s orbitals in the HOMO and LUMO[18,19] (see Fig. S3.1). The LUMO is a mixed metal–ligand orbital. It has

Table 2 Summary of the photoluminescent data of **1a–6a** (NO_3^- counterions) and **1b–6b** (SbF_6^- counterions) in the solid-state

Complex	Emission (nm)	Excitation (nm)	Quantum yield (%)	Average lifetime (μs)	Au···Au distance (Å)
1a	552	385	3.5	2.18	
1b	430	364, 395	29	1.26	2.7884(6)
1c	586	410	11.7	3.39	2.863(1)
2a	540	384	2.9	2.00	
2b	431	363, 395	0.8	0.18	2.7537(3)
3a	540	385	4.5	2.22	
3b	432	365, 403	2.6	0.25	2.7575(7)
4a	540	380	4.7	2.38	
4b	430	365, 400	10	0.65	2.7812(3)
5a	540	385	4.4	2.41	
5b	434	366, 406	3.4	0.32	2.7752(3)
6a	546	381	2.6	2.45	
6b	435	363, 407	0.7	0.45	2.789[a]

[a] The value was taken from a DFT calculation at the TPSSh-D3BJ/def2TZVP level because the crystal structure was not obtained.

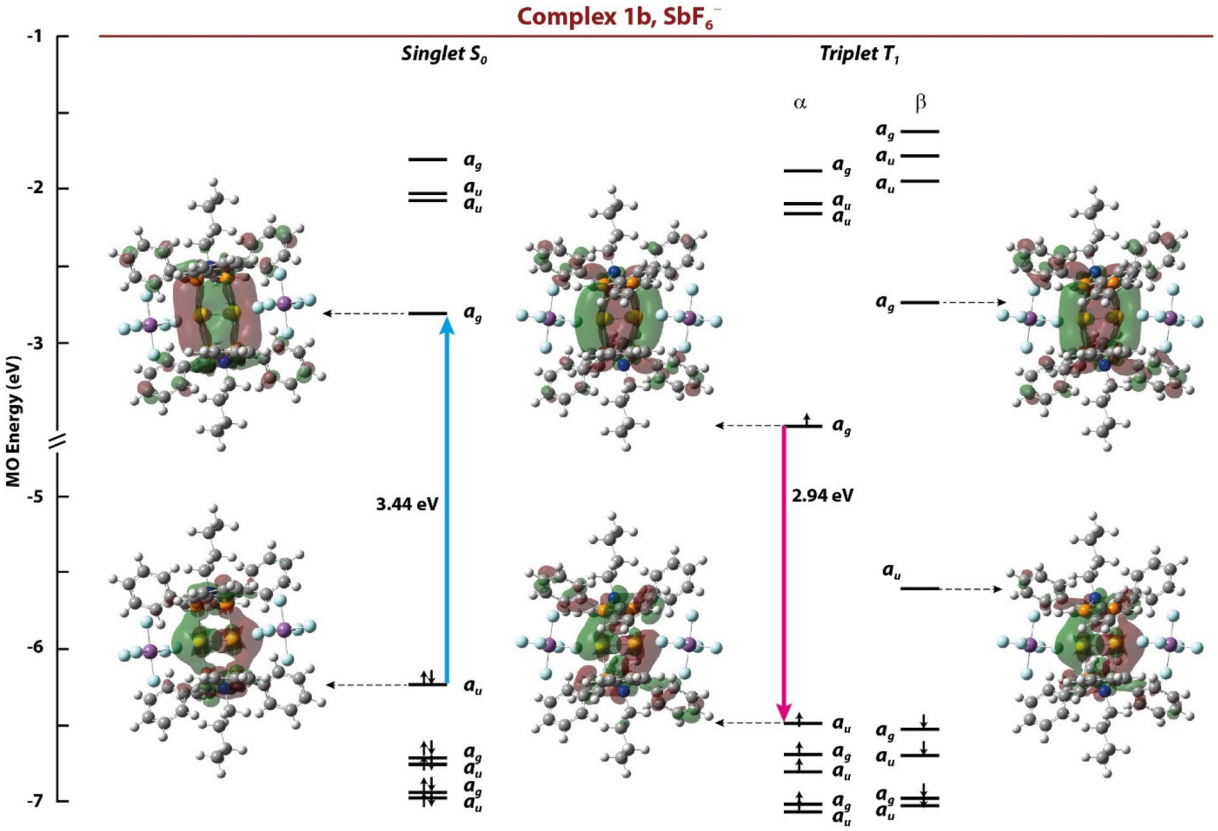

Fig. 6 Frontier molecular orbitals (MOs) of **1b** calculated at the TPSSh level for the singlet ground state and the first triplet excited state (T_1). The blue arrow indicates the $S_0 \rightarrow S_1$ absorption transition and the red arrow describes the $S_0 \leftarrow T_1$ emission transition.

large contributions from the p and d orbitals of P and N, and smaller contributions from the s and p orbitals of the Au atoms. The LUMO shows an Au–P bonding, and Au–Au bonding character. The HOMO–LUMO gaps calculated at the TPSSh level are 3.44 eV and 3.46 eV, for R = *n*Bu and 2,6Me, respectively. Significantly larger gaps of 4.11 eV and 4.16 eV, respectively, have been calculated for the two complexes at the B3LYP level. The latter value is close to the literature value of 4.06 eV calculated for the same complex with R = 2,6Me using the B3LYP functional (without counterions).[43] Despite the different R groups and Au···Au distances, the theoretically predicted absorption and emission properties are quite similar for these two complexes with SbF_6^- counterions. The TPSSh values are discussed below, while the B3LYP values are given in Table 3. Overall, the TPSSh functional consistently shows better agreement with the experimental photophysical studies

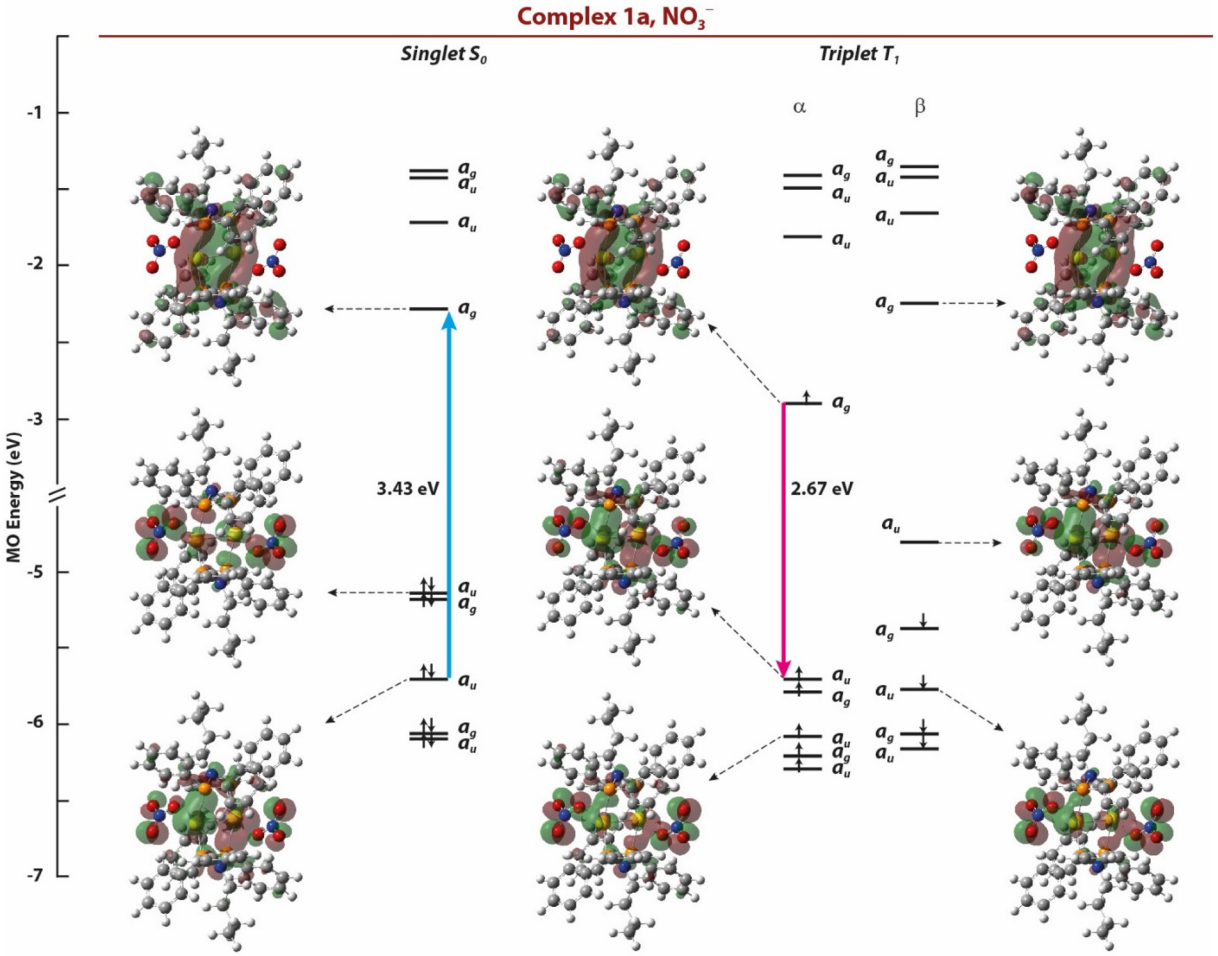

Fig. 7 Frontier molecular orbitals (MOs) of **1a** calculated at the TPSSh level for the singlet ground state and the first triplet excited state (T_1). The blue arrow indicates the $S_0 \rightarrow S_5$ absorption transition and the red arrow describes the $S_0 \leftarrow T_1$ emission transition.

than B3LYP for both excitation and emission transitions. This is in line with a much better agreement of the Au···Au distances calculated with the TPSSh functional with the experimental values (within 0.02 Å). In contrast, the Au···Au distances calculated with the B3LYP functional exhibit a deviation of 0.03 Å–0.06 Å, see Table 3. The theoretically calculated TPSSh absorption spectra for the complexes with R = *n*Bu and different counterions are shown in Fig. 9. For complex **1b** (R = *n*Bu, SbF_6^-) the two lowest allowed theoretically predicted absorption bands are at 381 nm, and 335 nm, respectively (Table 3). The lowest energy and most intense transition calculated at the TPPSh level is in very good agreement with one of the experimental excitation wavelengths (395 nm). This band corresponds to a HOMO–LUMO transition. It is assigned to a mixture of ^{1}[sdσ* → spσ] metal-to-metal (MMCT) and metal-metal (sdσ*) to ligand (PNP) charge transfer (MMLCT). The second lowest allowed transition (at 335 nm) is from HOMO−2 to LUMO. HOMO−2 is centered on the phenyl rings of the PNP ligands. For the complex with R = 2,6Me, the lowest and most intense energy band was calculated to be at 378 nm and two other much weaker bands at 355 nm and 329 nm (Table 3). These values are in good agreement with the photophysical measurements of the previous work[43] (R = 2,6Me, absorption at 370 nm–380 nm and 322 nm).

The NO_3^- counterions are electron donors due to oxygen lone pairs and interact more strongly with the gold atoms than SbF_6^-, especially in the excited triplet state. In comparison to complex **1b** with SbF_6^- counterions, complex **1a** (R = *n*Bu, NO_3^- counterions) had a considerable increase of the Au···Au distance in both the ground and excited states by 0.06 Å and 0.11 Å, respectively (Table 3) and a slight redshift of the main absorption band. The MOs of the nitro groups are high in energy, slightly above the metal-centered sdσ* orbital, which becomes HOMO−2 in **1a**, while HOMO and HOMO−1 are now centered on the NO_3^- counterions (lone pairs of oxygens), see Fig. 7.

For complexes **1a** and **1b** (with R = *n*Bu), the experimental luminescence lifetimes measured in this work are in the order of microseconds, indicating the phosphorescent nature of the transitions.[51] However, since in the previous study of complexes with aromatic *N*-substituents the emissions were interpreted as fluorescence,[43] we calculated not only phosphor-

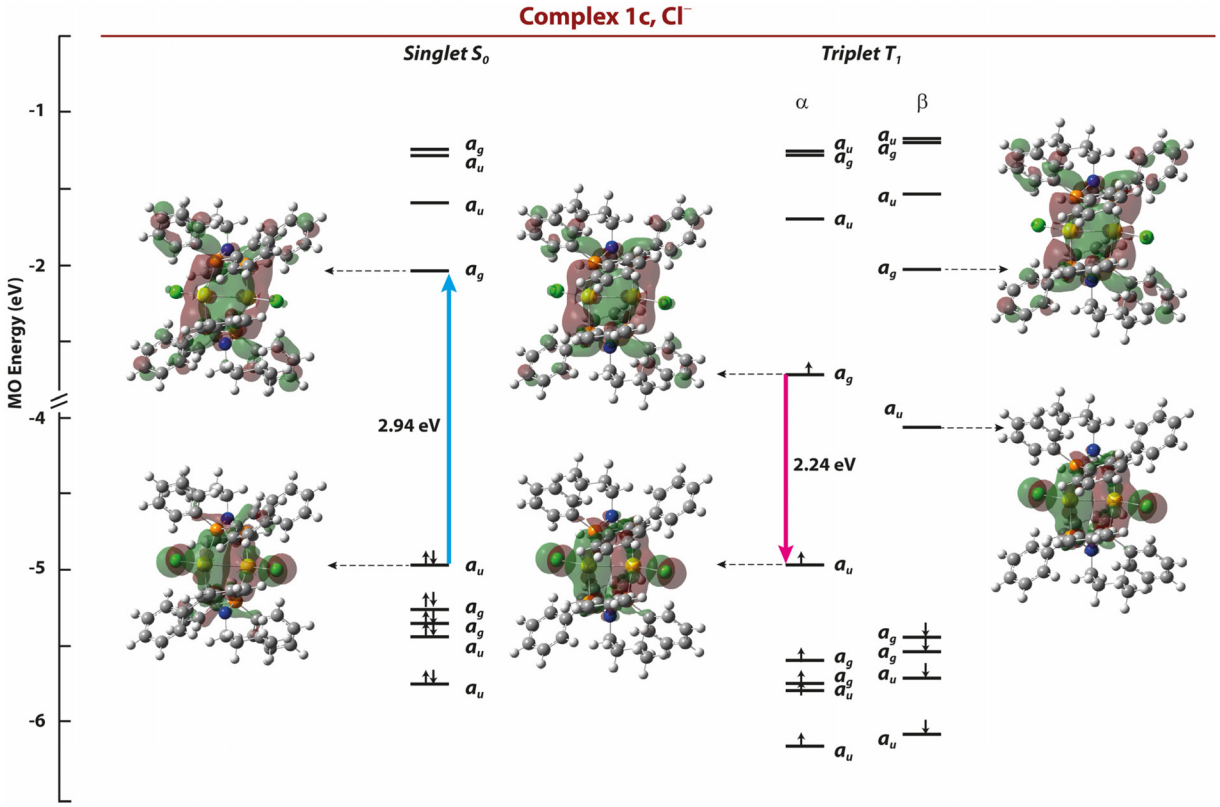

Fig. 8 Frontier molecular orbitals (MOs) of **1c** calculated at the TPSSh level for the singlet ground state and the first triplet excited state (T_1). The blue arrow indicates the $S_0 \rightarrow S_1$ absorption transition and the red arrow describes the $S_0 \leftarrow T_1$ emission transition.

escence but also possible fluorescence emission transitions ($S_0 \leftarrow S_1$ and $S_0 \leftarrow S_5$). We will first focus our discussion on the emission of complexes with SbF_6^- anions and then explain how the picture changes when SbF_6^- anions are exchanged for NO_3^- or Cl^-.

To calculate the emission spectra, we optimized the lowest triplet and singlet excited states of the complexes. We find that the Au···Au distances in the triplet state of the complexes are significantly shortened by 0.13 Å–0.17 Å with respect to the ground state at both B3LYP and TPSSh levels, see Table 3, so that a covalent Au–Au bond is formed in the T_1 excited state (and also in the S_1 state). This is attributed to the significant Au–Au σ bonding character of the LUMO (with the contribution of the Au 6p and 5s bonding combination directed along the Au···Au axis), which becomes occupied in the first triplet and singlet excited states. Such shortening of the aurophilic Au···Au contacts in the excited state is well established.[49] The resulting molecular distortion in the excited state appears to be responsible for the significant redshift in emission energy of gold complexes. In the triplet geometry, the energy separation between α-HOMO and α-HOMO−1 for complex **1b** decreases to 2.94 eV at the TPSSh level, see Fig. 6. We obtained the emission spectrum by using the TD-DFT approach and by calculating vertical singlet–triplet (and singlet–singlet) excitations from the singlet ground state in the optimized geometry of the respective excited state.

The T_1 state corresponds to a HOMO–LUMO excitation in the complexes with SbF_6^- counterions $^3[sd\sigma^* \rightarrow sp\sigma]$ and has an orbital composition similar to the S_1 state (Fig. S3.1). Therefore, T_1 is likely to be the emitting state. For **1b** (with R = *n*Bu and SbF_6^- counterions), the TPSSh functional predicts a slightly overestimated emission wavelength for the $S_0 \leftarrow T_1$ transition at 483 nm (experimental value is 430 nm), Table 3. Alternatively, if S_1 is emitting, the theoretically predicted emission wavelength at 417 nm is quite close to the experimental value. However, the measured emission lifetime of 1.26 μs suggests that the emission originates from the T_1 state.

The experimental measurements showed that the replacement of SbF_6^- by NO_3^- counterions has a significant effect on the emission wavelength, redshifting it from about 430 nm to 540 nm–550 nm. Abnormally large Stoke's shifts between the absorption spectrum and the emission have been previously reported for certain luminescent gold complexes, and this phenomenon has been explained by the formation of a so-called 'exciplex' (an adduct of the excited state with counterions or with the solvent molecules).[18,19,33–35] Our theoretical analysis shows a similar interaction of NO_3^- ions with the complex. The oxygen lone pairs of the NO_3^- groups in **1a** lie high in energy and their combination of A_{1u} symmetry interacts with the metal-based sdσ* MO to form two combinations (HOMO and HOMO−2) shown in Fig. 7. In the ground state, it is the HOMO−2 that has a higher metal–metal sdσ* character,

Table 3 Calculated absorption and emission transitions[a] for $[Au_2\{\mu_2\text{-}P(Ph)_2N(R)P(Ph)_2\}_2][SbF_6]_2$ complexes with R = *n*-butyl and 2,6-dimethylphenyl compared to the experimental values

	Absorption			Absorption			Au···Au distance (Å)		
	Wavelength (nm)			Wavelength (nm)					
Complex	Theory[c]	Expt[d]	Type of transition	Theory[c]	Expt[d]	Type of transition[b]	S_0	T_1	S_1
R = *n*Bu, SbF_6^- (**1b**)	381 (0.2032)	395	$S_0 \rightarrow S_1$	483	430	$[T_1]$: $S_0 \leftarrow T_1$	2.805	2.679	2.705
	350 (0.2260)		HOMO → LUMO	*430*		HOMO ← LUMO	*2.847*	*2.683*	*2.724*
							Expt		
							2.788		
	335 (0.0649)	364	$S_0 \rightarrow S_3$	417		$[S_1]$: $S_0 \leftarrow S_1$			
	309 (0.0710)		HOMO−2 → LUMO	*372*		HOMO ← LUMO			
R = *n*Bu, NO_3^- (**1a**)	484 (0.0154)		$S_0 \rightarrow S_1$	567	552	$[T_1]$: $S_0 \leftarrow T_1$	2.867	2.788	
	412 (0.0379)		HOMO → LUMO	*482*		HOMO ← LUMO	*2.966*	*2.792*	
						HOMO−2 ← LUMO			
	389 (0.1108)	385	$S_0 \rightarrow S_5$ (S_3)	476		$[T_3]$: $S_0 \leftarrow T_3$			
	350 (0.1120)		HOMO−2 → LUMO	*435*		HOMO−2 ← LUMO			
						HOMO ← LUMO			
	352 (0.0421)		$S_0 \rightarrow S_{10}$	427		$[S_1]$: $S_0 \leftarrow S_5$			
			HOMO−4 → LUMO			HOMO−2 ← LUMO			
R = *n*Bu, Cl^- (**1c**)	463 (0.0725)	410	$S_0 \rightarrow S_1$	712	586	$[T_1]$: $S_0 \leftarrow T_1$	2.912	2.754	
	425 (0.0805)		HOMO → LUMO	*457*		HOMO ← LUMO	*2.967*	*2.782*	
							Expt		
							2.863		
	401 (0.0112)		$S_0 \rightarrow S_4$						
	365 (0.0144)		HOMO−4 → LUMO						
	367 (0.0129)		$S_0 \rightarrow S_6$						
			HOMO → LUMO+1						
R = 2,6Me, SbF_6^-	378 (0.1736)	383[e]	$S_0 \rightarrow S_1$	476	423, 497[e]	$[T_1]$: $S_0 \leftarrow T_1$	2.826	2.670	2.719
	347 (0.1989)		HOMO → LUMO	*418*		HOMO ← LUMO	*2.862*	*2.689*	
							Expt		
							2.830[e]		
	355 (0.0055)	322[e]	$S_0 \rightarrow S_3$	407	423, 497[e]	$[S_1]$: $S_0 \leftarrow S_1$			
	317 (0.0063)		HOMO−2 → LUMO	*379*		HOMO ← LUMO			
	329 (0.0039)		$S_0 \rightarrow S_5$						
	297 (0.0238)		HOMO−4 → LUMO						

[a] Only transitions of A_{1u} symmetry are listed. [b] A notation of the type $[T_1]$: $S_0 \leftarrow T_1$ means that we have computed vertical $S_0 \rightarrow T_1$ excitations at the geometry of a triplet state T_1, which should correspond to $S_0 \leftarrow T_1$ emission. [c] B3LYP values are given in italic and TPSSh values in a regular font. Oscillator strengths are given in parentheses. [d] We compare to the experimental excitation spectra. [e] Data from ref. 43.

and a transition from this orbital to the LUMO corresponds to the main absorption band, $S_0 \rightarrow S_5$ (or $S_0 \rightarrow S_3$ at the B3LYP level). Notably, the energy gap between the HOMO−2 and the LUMO is essentially the same as the HOMO–LUMO gap in **1b**, explaining why the absorption wavelength is not significantly affected by the counterion exchange. This excited singlet state of $^1[sd\sigma^* \rightarrow sp\sigma]$ nature is similar in composition and is expected to cross with two low-lying triplet states of A_{1u} symmetry, T_1 and T_3. Both involve mixed HOMO → LUMO and HOMO−2 → LUMO transitions of the type ^{3}[nitrate → spσ] and $^3[sd\sigma^* \rightarrow sp\sigma]$, where HOMO and LUMO refer to the singlet-state MOs. The Au···O contacts (with oxygens of the nitrate ions) get notably stretched in T_3 and in S_5 from 2.48 Å in the ground state to 2.62 Å in T_3 and to 2.54 Å in S_5. This is because an electron is removed from the HOMO−2 orbital with partially Au···O bonding character, destabilizing the Au···O interaction. The Au–Au bond is weaker in the T_1 and T_3 excited states of nitrate complexes compared to hexafluoroantimonate complexes, which is reflected in a longer Au···Au distance in T_1 of **1a** (2.79 Å) than in T_1 of **1b** (2.68 Å), Table 3. Interestingly, in the T_1 excited state optimized by conventional unrestricted DFT, the original HOMO and HOMO−2 are swapped, see Fig. 7, consistent with the mixed nature of the transition involving both HOMO and HOMO−2. The T_1 state is calculated to emit at 567 nm, which agrees well with the experimentally measured emission at 552 nm, and a higher energy T_3 state is predicted to emit at 476 nm. The latter transition was not observed experimentally. The calculated $S_0 \leftarrow S_5$ transition has an even shorter wavelength, so only the $S_0 \leftarrow T_1$ assignment agrees well with the experimental value.

The change in the luminescent properties as a result of interaction with nitrate ions is an interesting effect which inspired us to also look at the even stronger interacting counterion, chloride. We therefore studied the photophysical properties of the complex analogous to **1a** and **1b** with two Cl^- counterions (denoted **1c**) both experimentally and computationally.

In the ground state of **1c** (S_0), the computed TPSSh Au···Au distance is 2.91 Å, even longer than in the nitrate complex,

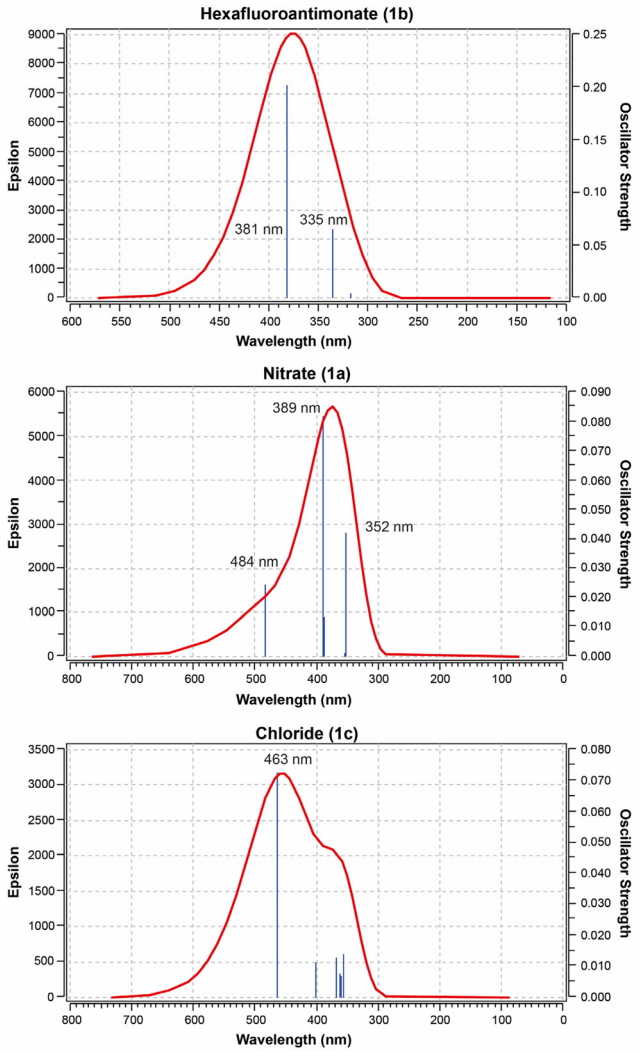

Fig. 9 Theoretically predicted (TPSSh) UV/Vis absorption spectra of **1b**, **1a**, and **1c** (with R = *n*Bu and SbF_6^-, NO_3^-, or Cl^- counterions, respectively).

whereas the Au···Cl distances are 2.56 Å, which is close to the sum of covalent radii of Au and Cl and is indicative of a bond with a significant covalent character. The MOs of the ground state are qualitatively similar to **1b**, but showing a reduced HOMO–LUMO gap of 2.94 eV, with another notable difference that the HOMO includes large contributions from the p orbitals of the Cl^- ions interacting with Au in an antibonding fashion (Fig. 8). This explains further shortening of the Au···Cl contacts to 2.52 Å in the T_1 state (as opposed to elongation of Au···O in the nitrate complexes). The Au···Au distance shortens to 2.75 Å in the T_1 state, even shorter than in the case of the nitrate complex. This large geometry change from ground to excited state is probably responsible for the large Stoke's shift between the absorption and the emission transitions. The experimentally measured excitation and emission wavelengths are 410 and 586 nm (respectively), *i.e.* the emission is significantly redshifted with respect to the SbF_6^- complex **1b** (430 nm). The computed (TPSSh) absorption and emission wavelengths (463 nm and 712 nm, respectively) are significantly overestimated, but qualitatively they confirm the trend of increasing the emission wavelength in the order SbF_6^- < NO_3^- < Cl^-.

In summary, our computational analysis of the absorption and emission transitions in two representative dinuclear Au(I) complexes with aromatic and aliphatic *N*-substituents on the PNP ligand and with weakly interacting SbF_6^- counterions revealed minimal variation in the absorption and emission wavelengths, despite slightly different Au···Au distances in these complexes. This finding aligns with the very similar photophysical properties found experimentally for the studied complex series. Notably, changing the counterion from SbF_6^- to NO_3^- or to Cl^- shifts the absorption and especially the emission wavelengths to lower energies. In the case of NO_3^-, our computational analysis attributes this effect to the different atomic orbital compositions of the HOMO in the nitrate and hexafluoroantimonate complexes. The HOMO orbital of the nitrate complexes is mainly composed of the oxygen lone pairs of the NO_3^- groups, positioned above the Au···Au sdσ* orbital HOMO−2 (which serves as the HOMO in the hexafluoroantimonate complexes). This sdσ* orbital is responsible for the main electronic transition. The resulting singlet excited state has an orbital composition and structure resembling both the T_1 and T_3 states, each with some ^{3}[sdσ* → spσ] character. Importantly, the predicted $T_1 \rightarrow S_0$ emission transition in the nitrate complex aligns well with experimental observations regarding its low energy. In the case of Cl^-, the nature of the HOMO and LUMO is similar to that in the weakly interacting SbF_6^- complex, however, the HOMO includes large contributions from the Cl ions. In the excited state geometry with much reduced Au···Au distance, the former significantly rises in energy, reducing the HOMO–LUMO gap and the energy of the emission transition.

Conclusions

In this study, we explored the feasibility of tuning the geometry and photoluminescence of fully supported dinuclear di-gold(I) complexes by modifying the *N*-substituents on the phosphinoamine-based (PNP) chelating ligand and altering the counterions within the crystal structure.

We successfully synthesized and characterized six bis(μ_2-bis(diphenylphosphino)-amine)-di-gold(I) nitrate complexes with different *N*-substituents. By substituting nitrate counterions with hexafluoroantimonate counterions, six bis(μ_2-bis(diphenylphosphino)-amine)-di-gold(I) hexafluoroantimonate complexes were isolated and characterized. Four of the latter yielded crystal structures. Next, we conducted a comprehensive photoluminescence study on all twelve of the isolated complexes. Finally, the photophysical characteristics of selected representative complexes were investigated computationally and the results were compared to data obtained in the experimental study.

Notably, we observed that changes in geometry, and in particular the Au···Au distance resulting from the variation of the *N*-substituents on the PNP ligands, do not significantly alter the emission properties. Surprisingly, the counterions emerged as influential factors. We found that different counterions significantly affected the photophysical properties of these complexes. Computational TD-DFT studies played a crucial role in our investigation. By analyzing photoluminescence and molecular orbital characteristics, we gained insights into the electronic transitions within these luminescent complexes and provided a plausible explanation for the effect of counterions on the emission wavelength.

Our work provides a better understanding of the factors that influence the photoluminescence of dinuclear gold(I) complexes. These insights pave the way for further exploration and design of luminescent materials with tailored properties. In future work, we will explore other metal centers and *N*-substituents to further tune these properties and design novel luminescent materials.

Experimental section

Computational methods and models

The geometry optimizations of the bis(μ_2-PNP)-di-gold(I) complexes were performed using two hybrid density functionals, B3LYP[52–54] and TPSSh.[55] The def2TZVP basis set of Ahlrichs and Weigend[56,57] was used, which is a combination of a TZVP basis for main-group elements and a triple-zeta quality relativistic ECP for inner electronic shells of Au with the corresponding energy-optimized all electron basis set for the valence electrons. The same basis set was used for both geometry optimizations and TD-DFT calculations. Grimme's D3 dispersion correction with Becke-Johnson damping (DFT-D3BJ)[58,59] was added to the TPSSh and B3LYP functionals. The calculations were performed using Gaussian 16 software suite.[60]

For the chloride and hexafluoroantimonate derivatives, the initial counterions positions were taken directly from the experimental X-ray structures, and the complexes were then fully optimized with all atoms allowed to relax. For the nitrate complexes, where no crystallographic data were available, the initial geometries were generated by replacing SbF_6^- with NO_3^- in the corresponding hexafluoroantimonate structures. These geometries were then fully optimized in both ground and excited states. We are aware that this procedure represents an approximation, since packing effects in the solid state may influence the cation–anion arrangement and distances. Nonetheless, this strategy was adopted as a pragmatic way to include counterion effects consistently across the series. Importantly, test calculations revealed that in the presence of the SbF_6^- counterions slightly shorter Au···Au distances were obtained than without the inclusion of any counterions, in better agreement with experiment, whereas NO_3^- and Cl^- counterions exert a significant stretching effect on the Au···Au distances. While we recognize that this model cannot capture all possible packing-induced variations, it provides a physically reasonable description of the counterion influence and reproduces the main experimental trends. All geometry optimizations have been performed under C_i symmetry constraints. Cartesian coordinates of the complexes in the ground and excited states are listed in the Supplementary Computational Information (S3).

The first triplet excited states of the complexes (T_1) were optimized using standard unrestricted DFT calculations with the spin state fixed to triplet. The absorption spectra and $S_0 \leftarrow T_1$ emission transitions were calculated using single-point TD-DFT calculations at the S_0 and T_1 optimized geometries, respectively. The geometries of the excited singlet and higher triplet excited states were optimized by TD-DFT, which allowed the calculation of the corresponding emission wavelengths. Representations of molecular orbitals were plotted using the GaussView software[61] and the orbital compositions/populations were obtained using the Ros-Schuit partitioning (SCPA)[62] method, implemented in the Multiwfn program,[63] and an in-house Python script.

X-ray crystallography: collection and refinement details

All the complexes yielded colorless crystals. The crystallographic data for complexes **1b**, **2b**, **4b**, and **5b** were collected using a Bruker D8 Quest Eco Chi Photon II diffractometer, also equipped with a graphite monochromated MoK(α) radiation source with a wavelength of 0.71073 Å.

Unless otherwise stated, all data were collected at 100 K using phi and omega scans. SAINT-Plus software was used for data reduction and cell refinement, while absorption corrections were performed using the SADABS software with the multi-scan functionality.[64,65] SHELXT and SHELXL-2013 were used for structure solution and refinement, respectively, in conjunction with the WINGX and OLEX software systems.[66–69] Graphical depictions of molecular structures were created using DIAMOND.[70] All atoms, except hydrogen atoms, were anisotropically refined with thermal ellipsoids drawn at 50% probability. CheckCIFs were performed for all the crystal structures, with all A and B alerts corrected or explained. Additional crystallographic tables not included in this manuscript can be found in the SI. The Crystal Information Files (CIFs) for structures **1b**, **2b**, **4b**, **5b** have been submitted to the Cambridge Crystallographic Data Centre with CCDC deposition numbers of 2096913 (**1b**), 2091265 (**2b**), 2091263 (**4b**), and 2091267 (**5b**), respectively.

Physical methods

The ^{31}P, and ^{1}H NMR spectra were collected on a Bruker 400 MHz spectrometer in deuterated chloroform. Chemical shifts (^{1}H NMR) are reported in ppm relative to the TMS peak, Xi scale calibration was done for the ^{31}P NMR. The infrared spectra were measured using a Bruker Tensor Standard System spectrometer (ATR) with a range of 4000 to 370 cm^{-1}. The UV/Vis analysis was performed in DCM using a Varian Cary 50 Spectrometer in a 1.000(1) cm quartz cuvette. The solid-state photoluminescent studies were performed using an

Edinburgh Instruments FLS980 series fluorescence spectrometer. Samples were excited by a 450 W continuous wavelength xenon lamp (Xe1) filtered by a double monochromator. A 0.3 mm demountable quartz cuvette was used for the solid-state samples; the sample was uniformly packed across the surface of the cuvette. The same cuvette was used during the determination of the lifetime, for which samples were exposed to a pulsing LED source. [The emission bandwidth was adjusted so that the counting rate was less than 5% of the excitation rate, to ensure pulse pileup for the detector was negligible.] The determination of the quantum yield was done using an integrating sphere accessory. The Absolute Quantum Yield was determined by measuring a 100% reflection of the light source at a specific wavelength. Subsequently, the samples were exposed to the same light source at the same wavelength. The number of reflections were compared to that of the initial reflections to obtain a proportional value to the number of absorbed photons. Additionally, the fluorescence was measured to obtain a value proportional to the number of emitted photons and the ratio of these values gave the absolute yield. The lifetime was determined by exposing the complexes to a pulsing light source. By doing this we know that the lifetime observed is for one electron transition only. A decay curve was obtained by time correlated single photon counting. The time between the excitation and photon detection is measured and the data are fitted to obtain the lifetime.

Synthesis and characterization

All the synthetic procedures were performed in an inert (N_2) and dry atmosphere using a Schlenk line. All solvents were dried and distilled using known methods.[71] The chemicals were purchased from Sigma-Aldrich.

General procedure for the synthesis of the PNP ligands

In a typical reaction the primary amine (1 equivalent) was added to dichloromethane (20 mL) and triethylamine (3 equivalents). Chlorodiphenylphosphine (2 equivalents) was added dropwise while stirring the reaction mixture in an ice bath; 30 minutes after the addition, the ice bath was removed. The reaction was left to stir at room temperature for 48 h. The solution was filtered, and a white powder was isolated from the filtrate.

***n*ButylPNP (L1).** Butylamine (1 ml, 0.01 mol), chlorodiphenylphosphine (3.7 ml, 0.02 mol), triethylamine (4.21 ml, 0.03 mol). Yield: 4.04 g, 92%. Anal. calc. for $P_2N_1C_{28}H_{29}$: C, 76.17; H, 6.02; N, 3.17%. Found: C, 76.49; H, 5.89; N, 3.01%. ^{1}H NMR ($CDCl_3$, 400.13 MHz): δ 0.6 (t, 3H, CH_3, J = 7.24 Hz), 0.9–1.0 (m, 2H, CH_2), 1.0–1.1 (m, 2H, CH_2), 3.2–3.3 (m, 2H, CH_2), 7.2–7.5 (m, 20H, Ar H). $^{31}P\{^1H\}$ NMR ($CDCl_3$, 161.97 MHz): δ 62.1 (s). IR(ATR) ν (cm^{-1}): 2858–3069 (C–H (Ar)), 1433 (N–P), 1061 (N–C). UV/Vis: λ_{max} = 270 nm, ε = 4797 M^{-1} cm^{-1}.

***c*ButylPNP (L2).** Cyclobutylamine (0.6 ml, 0.007 mol), chlorodiphenylphosphine (2.6 ml, 0.014 mol), triethylamine (3 ml, 0.021 mol). Yield: 2.9 g, 94%. Anal. calc. for $P_2N_1C_{28}H_{27}$: C, 76.52; H, 6.19; N, 3.19%. Found: C, 76.78; H, 5.81; N, 3.49%. ^{1}H NMR ($CDCl_3$, 400.13 MHz): δ 1.3–1.4 (m, 2H, CH_2), 1.7–1.8 (m, 2H, CH_2), 2.4–2.6 (m, 2H, CH_2), 3.9–4.0 (m, 1H, CH), 7.2–7.8 (m, 20H, Ar). $^{31}P\{^1H\}$ NMR ($CDCl_3$, 161.97 MHz): δ 48.9 (s). IR (ATR) ν (cm^{-1}): 2842–3070 (C–H (Ar)), 1432 (N–P), 1089 (N–C). UV/Vis: λ_{max} = 268 nm, ε = 4251 M^{-1} cm^{-1}.

***c*PentylPNP (L3).** Cyclopentylamine (1 ml, 0.01 mol), chlorodiphenylphosphine (3.7 ml, 0.02 mol), triethylamine (4.21 ml, 0.03 mol). Yield: 2.17 g, 42%. Anal. calc. for $P_2N_1C_{29}H_{29}$: C, 76.81; H, 6.45; N, 3.09%. Found: C, 77.03; H, 6.76; N, 3.42%. ^{1}H NMR ($CDCl_3$, 400.13 MHz): δ 1.3 (s, 2H, CH_2), 1.5 (s, 2H, CH_2), 1.7 (s, 2H, CH_2), 1.9 (s, 2H, CH_2), 3.7–3.9 (m, 1H, CH), 7.2–7.8 (m, 20H, Ar). $^{31}P\{^1H\}$ NMR ($CDCl_3$, 161.97 MHz): δ 50.1 (s). IR (ATR) ν (cm^{-1}): 2861–3070 (C–H (Ar)), 1432 (N–P), 1089 (N–C). UV/Vis: λ_{max} = 266 nm, ε = 5373 M^{-1} cm^{-1}.

***c*HexylPNP (L4).** Cyclohexylamine (1.1 ml, 0.01 mol), chlorodiphenylphosphine (3.7 ml, 0.02 mol), triethylamine (4.21 ml, 0.03 mol). Yield: 2.32 g, 50%. Anal. calc. for $P_2N_1C_{30}H_{31}$: C, 77.32; H, 6.68; N, 3.00%. Found: C, 77.32; H, 6.27; N, 3.27%. ^{1}H NMR ($CDCl_3$, 400.13 MHz): δ 0.9–1.0 (m, 2H, CH_2), 1.3–1.4 (m, 2H, CH_2), 1.4–1.5 (m, 4H, 2 × CH_2), 1.7–1.9 (m, 2H, CH_2), 3.1–3.2 (m, 1H, CH), 7.2–7.8 (m, 20H, Ar). $^{31}P\{^1H\}$ NMR ($CDCl_3$, 161.97 MHz): δ 49.6 (s). IR (ATR) ν (cm^{-1}): 2849–3069 (C–H (Ar)), 1450 (N–P), 1056 (N–C). UV/Vis: λ_{max} = 269 nm, ε = 4564 M^{-1} cm^{-1}.

2-ButylPNP (L5). 2-Butylamine (1.0 ml, 0.01 mol), chlorodiphenylphosphine (3.7 ml, 0.02 mol), triethylamine (4.2 ml, 0.03 mol). Yield: 2.36 g, 53%. Anal. calc. for $P_2N_1C_{28}H_{29}$: C, 76.17; H, 6.62; N, 3.17%. Found: C, 76.08; H, 7.00; N, 3.45%. ^{1}H NMR ($CDCl_3$, 400.13 MHz): δ 0.7 (t, 3H, CH_3, J = 7.54 Hz), 1.2 (d, 3H, CH_3, J = 6.43 Hz), 1.7–1.8 (m, 1H, CH_2), 3.3–3.4 (m, 1H, CH), 7.3–7.4 (m, 20H, Ar). $^{31}P\{^1H\}$ NMR ($CDCl_3$, 161.97 MHz): δ 50.7 (s). IR (ATR) ν (cm^{-1}): 2862–3070 (C–H (Ar)), 1431 (N–P), 1090 (N–C). UV/Vis: λ_{max} = 268 nm, ε = 4785 M^{-1} cm^{-1}.

DIMPPNP (L6). 1,2-Dimethylpropylamine (1.2 ml, 0.01 mol), chlorodiphenylphosphine (3.7 ml, 0.02 mol), triethylamine (4.21 ml, 0.03 mol). Yield: 1.75 g, 38%. Anal. calc. for $P_2N_1C_{29}H_{31}$: C, 76.47; H, 6.86; N, 3.07%. Found: C, 76.32; H, 7.26; N, 3.28%. ^{1}H NMR ($CDCl_3$, 400.13 MHz): δ 0.5 (d, 3H, CH_3, J = 7.0 Hz), 0.9 (d, 3H, CH_3, J = 6.94 Hz), 1.3 (d, 3H, CH_3, 7.0 Hz), 1.4–1.5 (m, 1H, CH), 3.4–3.5 (m, 1H, CH_3), 7.2–7.7 (m, 20H, Ar). $^{31}P\{^1H\}$ NMR ($CDCl_3$, 161.97 MHz): δ 54.6 (s). IR (ATR) ν (cm^{-1}): 2868–3072 (C–H (Ar)), 1435 (N–P), 1096 (N–C). UV/Vis: λ_{max} = 270 nm, ε = 5770 M^{-1} cm^{-1}.

General procedure for the synthesis of the Au(I) nitrate complexes

In a typical reaction 1 eq. PNP ligand was added to 1 eq. [AuCl(Me_2S)] and stirred in DCM (20 mL) at room temperature for 24 hours. The solution was filtered and the solvent was removed under reduced pressure. The formation of the dimeric and/or monomeric precursor was confirmed using ^{31}P NMR. Different ratios of these precursors were observed for the different complexes and no definite trend between the steric bulk and ratio was established. For this study, the final product was the complex of interest and therefore the precur-

sors were not isolated as both precursors lead to the formation of the dimeric complex upon the addition of $AgNO_3$. A slight excess of $AgNO_3$ (slightly more than 1 eq.) was added to the precursors in DCM and stirred at room temperature overnight. The solution was filtered. The solvent was evaporated under reduced pressure and the product was isolated as a yellow powder.[43]

Bis(μ$_2$-bis(*n*ButylPNP)-di-gold(I)bis(nitrate)) (1a). ButylPNP (0.1008 g, 2.28×10^{-4} mol) [AuCl(Me_2S)] (0.0672 g, 2.28×10^{-4} mol) $AgNO_3$ (0.0412 g, 2.43×10^{-4} mol). Yield: 0.2865 g, 90%. Anal. calc. for $Au_2N_4P_4O_6C_{56}H_{58}$: C, 48.01; H, 4.17; N, 4.00; O, 6.85%. Found: C, 48.29; H, 4.06; N, 4.30; O, 6.47%. ^{1}H NMR ($CDCl_3$, 400.13 MHz): δ 0.2 (t, 6H, 2 × CH_3, J = 7.06 Hz), 0.4–0.5 (m, 8H, 4 × CH_2), 2.6–2.7 (m, 4H, 2 × CH_2), 7.4–7.8 (m, 40H, Ar H). ^{31}P{^{1}H} NMR ($CDCl_3$, 161.97 MHz): δ 95.1 (s). IR (ATR) ν (cm^{-1}): 2872–3056 (C–H (Ar)), 1260 (N–P), 1026 (N–C). UV/Vis: λ_{max} = 346 nm, ε = 32 354 M^{-1} cm^{-1}.

Bis(μ$_2$-bis(*c*ButylPNP)-di-gold(I)bis(nitrate)) (2a). cButylPNP (0.0996 g, 2.27×10^{-4} mol), [AuCl(Me_2S)] (0.0648 g, 2.20×10^{-4} mol), $AgNO_3$ (0.0419 g, 2.46×10^{-4} mol). Yield: 0.2093 g, 66%. Anal. calc. for $Au_2N_4P_4O_6C_{56}H_{54}$: C, 48.15; H, 3.90; N, 4.01; O, 6.87%. Found: C, 48.25; H, 4.25; N, 3.78; O, 6.62%. ^{1}H NMR ($CDCl_3$, 400.13 MHz): δ 0.9–1.1 (m, 4H, 2 × CH_2), 1.3–1.4 (m, 4H, 2 × CH_2), 1.5–1.6 (m, 4H, 2 × CH_2), 4.0–4.1 (m, 2H, 2 × CH), 7.5–7.7 (m, 40H, Ar). ^{31}P{^{1}H} NMR ($CDCl_3$, 161.97 MHz): δ 95.7 (s). IR (ATR) ν (cm^{-1}): 2807–2960 (C–H (Ar)), 1304 (N–P), 1062 (N–C). UV/Vis: λ_{max} = 349 nm, ε = 28 646 M^{-1} cm^{-1}.

Bis(μ$_2$-bis(*c*PentylPNP)-di-gold(I)bis(nitrate)) (3a). *c*PentylPNP (0.1013 g, 2.23×10^{-4} mol) [AuCl(Me_2S)] (0.0681 g, 2.31×10^{-4} mol) $AgNO_3$ (0.0426 g, 2.51×10^{-4} mol). Yield: 0.2192 g, 69%. Anal. calc. for $Au_2N_4P_4O_6C_{58}H_{58}$: C, 48.89; H, 4.10; N, 3.93; O, 6.74%. Found: C, 48.75; H, 4.27; N, 4.29; O, 6.89%. ^{1}H NMR ($CDCl_3$, 400.13 MHz): δ 0.6–0.7 (m, 4H, 2 × CH_2), 0.8–0.9 (m, 4H, 2 × CH_2), 1.1–1.2 (m, 8H, 4 × CH_2), 3.9–4.0 (m, 2H, 2 × CH), 7.4–7.8 (m, 40H, Ar). ^{31}P{^{1}H} NMR ($CDCl_3$, 161.97 MHz): δ 94.8 (s). IR (ATR) ν (cm^{-1}): 2962–3055 (C–H (Ar)), 1260 (N–P), 1016 (N–C). UV/Vis: λ_{max} = 346 nm, ε = 26 812 M^{-1} cm^{-1}.

Bis(μ$_2$-bis(*c*HexylPNP)-di-gold(I)bis(nitrate)) (4a). *c*HexylPNP (0.1001 g, 2.14×10^{-4} mol) [AuCl(Me_2S)] (0.0655 g, 2.22×10^{-4} mol) $AgNO_3$ (0.0431 g, 2.54×10^{-4} mol). Yield: 0.2072 g, 67%. Anal. calc. for $Au_2N_4P_4O_6C_{60}H_{62}$: C, 49.60; H, 4.37; N, 4.13; O, 6.21%. Found: C, 50.00; H, 4.37; N, 4.13; O, 6.21%. ^{1}H NMR ($CDCl_3$, 400.13 MHz): δ 0.1–0.3 (m, 4H, 2 × CH_2), 0.5–0.6 (m, 8H, 4 × CH_2), 1.1–1.2 (m, 4H, 2 × CH_2), 2.0–2.2 (m, 4H, 2 × CH_2), 3.4 (m, 2H, 2 × CH), 7.2–7.7 (m, 40H, Ar). ^{31}P{^{1}H} NMR ($CDCl_3$, 161.97 MHz): δ 95.4 (s). IR (ATR) ν (cm^{-1}): 2852–3055 (C–H (Ar)), 1259 (N–P), 1018 (N–C). UV/Vis: λ_{max} = 345 nm, ε = 26 811 M^{-1} cm^{-1}.

Bis(μ$_2$-bis(2-ButylPNP)-di-gold(I)bis(nitrate)) (5a). 2-ButylPNP (0.0992 g, 2.25×10^{-4} mol) [AuCl(Me_2S)] (0.0694 g, 2.36×10^{-4} mol) $AgNO_3$ (0.0440 g, 2.59×10^{-4} mol). Yield: 0.2530 g, 78%. Anal. calc. for $Au_2N_4P_4O_6C_{56}H_{58}$: C, 48.01; H, 4.17; N, 4.00; O, 6.85%. Found: C, 47.78; H, 4.02; N, 4.32; O, 6.74%. ^{1}H NMR ($CDCl_3$, 400.13 MHz): δ 0.1–0.2 (m, 6H, 2 × CH_3), 0.4–0.5 (m, 2H, CH_2), 0.6–0.7 (m, 6H, 2 × CH_3), 1.0–1.1 (m, 2H, CH_2), 3.5–3.6 (m, 2H, 2 × CH), 7.4–7.8 (m, 40H, Ar). ^{31}P{^{1}H} NMR ($CDCl_3$, 161.97 MHz): δ 94.9 (s). IR (ATR) ν (cm^{-1}): 2873–3051 (C–H (Ar)), 1260 (N–P), 1096 (N–C). UV/Vis: λ_{max} = 345 nm, ε = 29 802 M^{-1} cm^{-1}.

Bis(μ$_2$-bis(DIMPPNP)-di-gold(I)bis(nitrate)) (6a). DIMPPNP (0.1004 g, 2.25×10^{-4} mol), [AuCl(Me_2S)] (0.0639 g, 2.17×10^{-4} mol) $AgNO_3$ (0.0449 g, 2.65×10^{-4} mol). Yield: 0.3187 g, 99%. Anal. calc. for $Au_2N_4P_4O_6C_{58}H_{62}$: C, 48.75; H, 4.37; N, 3.92; O, 6.72%. Found: C, 48.65; H, 4.75; N, 3.59; O, 6.34%. ^{1}H NMR ($CDCl_3$, 400.13 MHz): δ 0.1–0.2 (m, 12H, 4 × CH_3), 0.7–0.8 (m, 6H, 2 × CH_3), 1.0–1.1 (m, 2H, 2 × CH), 3.4–3.5 (m, 2H, 2 × CH), 7.3–7.9 (m, 40H, Ar). ^{31}P{^{1}H} NMR ($CDCl_3$, 161.97 MHz): δ 94.6 (s). IR (ATR) ν (cm^{-1}): 2873–3058 (C–H (Ar)), 1262 (N–P), 1094 (N–C). UV/Vis: λ_{max} = 345 nm, ε = 33 807 M^{-1} cm^{-1}.

Au(I) hexafluoroantimonate complexes

Complexes **1b–6b** were synthesized following a procedure analogous to that for **1a–6a** where 1 eq. of the PNP ligand was added to 1 eq. [AuCl(Me_2S)] in DCM (20 mL) and stirred at room temperature for 24 hours. The reaction mixture was filtered and the solvent was removed from the filtrate under reduced pressure. ^{31}P NMR was used to confirm the formation of both the dimeric and monomeric chlorido precursors in varying ratios. Since the dimeric product **1b–6b** was the complex of interest for this study the chlorido precursors were not isolated. Treatment of the precursor mixture with a slight excess (>1 eq.) of $AgSbF_6$ in DCM and stirring overnight at room temperature led to clean conversion to the desired dimeric complexes. After filtration to remove AgCl and evaporation of the solvent, the products were isolated as yellow powders. Crystals suitable for X-ray diffraction were obtained for **1b**, **2b**, **4b**, and **5b** by layering pentane over DCM solutions of the complexes.

Bis(μ$_2$-bis(*n*ButylPNP)-di-gold(I)bis(hexafluoroantimonate)) (1b). ButylPNP (0.1005 g, 2.28×10^{-4} mol), [AuCl(Me_2S)] (0.0663 g, 2.25×10^{-4} mol), $AgSbF_6$ (0.0790 g, 2.30×10^{-4} mol). Yield: 0.1164 g, 69%. Anal. calc. for $Au_2Sb_2F_{12}P_4N_2C_{56}H_{58}$: C, 38.47; H, 3.34; N, 1.60%. Found: C, 38.22; H, 3.52; N, 1.26%. ^{1}H NMR ($CDCl_3$, 400.13 MHz): δ 0.2–0.3 (t, 6H, 2 × CH_3, J = 7 Hz), 0.4–0.5 (m, 4H, 2 × CH_2), 0.5–0.6 (m, 4H, 2 × CH_2), 2.8–2.9 (m, 4H, 2 × CH_2), 7.3–7.9 (m, 40H, aromatic). ^{31}P{^{1}H} NMR ($CDCl_3$, 161.97 MHz): δ 96.0 (s) UV/Vis: λ_{max} = 304 nm, ε = 15 217 M^{-1} cm^{-1}.

Bis(μ$_2$-bis(*c*ButylPNP)-di-gold(I)bis(hexafluoroantimonate)) (2b). CyclobutylPNP (0.1008 g, 2.29×10^{-4} mol), [AuCl(Me_2S)] (0.0686 g, 2.33×10^{-4} mol), $AgSbF_6$ (0.0825 g, 2.4×10^{-4} mol). Yield: 0.1460 g, 84%. Anal. calc. for $Au_2Sb_2F_{12}P_4N_2C_{56}H_{54}$: C, 38.56; H, 3.12; N, 1.61%. Found: C, 38.69; H, 3.52; N, 2.00%. ^{1}H NMR ($CDCl_3$, 400.13 MHz): δ 1.0–1.1 (m, 4H, 2 × CH_2), 1.3 (s, 4H, 2 × CH_2), 1.4–1.5 (m, 4H, 2 × CH_2), 3.2–3.3 (m, 2H, 2 × CH), 7.3–8.0 (m, 40H, Ar). ^{31}P{^{1}H} NMR ($CDCl_3$, 161.97 MHz): δ 95.9 (s). UV/Vis: λ_{max} = 340, 310 nm, ε = 19 670, 14 436 M^{-1} cm^{-1}.

Bis(μ$_2$-bis(*c*PentylPNP)-di-gold(I)bis(hexafluoroantimonate)) (3b). CyclopentylPNP (0.1008 g, 2.22×10^{-4} mol), [AuCl(Me_2S)]

(0.0648 g, 2.20×10^{-4} mol), $AgSbF_6$ (0.0788 g, 2.30×10^{-4} mol). Yield: 0.1074 g, 64%. Anal. calc. for $Au_2Sb_2F_{12}P_4N_2C_{58}H_{58}$: C, 39.30; H, 3.30; N, 1.58%. Found: C, 38.96; H, 2.91; N, 1.87%. ^{1}H NMR ($CDCl_3$, 400.13 MHz): δ 0.7–0.8 (m, 4H, 2 × CH_2), 0.8–0.9 (m, 4H, 2 × CH_2), 1.1–1.3 (m, 8H, 4 × CH_2), 3.7–4.0 (m, 2H, 2 × CH), 7.3–7.9 (m, 40H, Ar). $^{31}P\{^1H\}$ NMR ($CDCl_3$, 161.97 MHz): δ 95.1 (s). UV/Vis: λ_{max} = 342 nm, ε = 22 935 M^{-1} cm^{-1}.

Bis(μ$_2$-bis(*c*HexylPNP)-di-gold(I)bis(hexafluoroantimonate)) (4b). CyclohexylPNP (0.1003 g, 2.15×10^{-4} mol), [AuCl(Me_2S)] (0.0631 g, 2.14×10^{-4} mol), $AgSbF_6$ (0.0770 g, 2.20×10^{-4} mol). Yield: 0.1122 g, 68%. Anal. calc. for $Au_2Sb_2F_{12}P_4N_2C_{60}H_{62}$: C, 40.03; H, 3.47; N, 1.56%. Found: C, 40.19; H, 3.60; N, 1.89%. ^{1}H NMR ($CDCl_3$, 400.13 MHz): δ 0.1–0.4 (m, 4H, 2 × CH_2), 0.6–0.9 (m, 8H, 4 × CH_2), 1.2–1.5 (m, 8H, 4 × CH_2), 3.6–3.8 (m, 2H, 2 × CH), 7.4–8.0 (m, 40H, Ar). $^{31}P\{^1H\}$ NMR ($CDCl_3$, 161.97 MHz): δ 96.3 (s). UV/Vis: λ_{max} = 330 nm, ε = 19 595 M^{-1} cm^{-1}.

Bis(μ$_2$-bis(2-butylPNP)-di-gold(I)bis(hexafluoroantimonate)) (5b). 2-butylPNP (0.1010 g, 2.29×10^{-4} mol), [AuCl(Me_2S)] (0.0668 g, 2.27×10^{-4} mol), $AgSbF_6$ (0.0797 g, 2.32×10^{-4} mol). Yield: 0.7308 g, 73%. Anal. calc. for $Au_2Sb_2F_{12}P_4N_2C_{56}H_{58}$: C, 38.47; H, 3.34; N, 1.60%. Found: C, 38.87; H, 2.95; N, 1.82%. ^{1}H NMR ($CDCl_3$, 400.13 MHz): δ 0.1–0.2 (m, 4H, 2 × CH_2), 0.8–0.9 (m, 6H, 2 × CH_3), 1.1–1.3 (m, 6H, 2 × CH_3), 3.6–3.8 (m, 2H, 2 × CH), 7.3–7.9 (m, 40H, Ar). $^{31}P\{^1H\}$ NMR ($CDCl_3$, 161.97 MHz): δ 95.9 (s). UV/Vis: λ_{max} = 310 nm, ε = 14 133 M^{-1} cm^{-1}.

Bis(μ$_2$-bis(DIMPPNP)-di-gold(I)bis(hexafluoroantimonate)) (6b). 1,2-DimethylpropylPNP (0.1004 g, 2.20×10^{-4} mol), [AuCl(Me_2S)] (0.0648 g, 2.20×10^{-4} mol), $AgSbF_6$ (0.0777 g, 2.26×10^{-4} mol). Yield: 0.7648 g, 76%. Anal. calc. for $Au_2Sb_2F_{12}P_4N_2C_{58}H_{62}$: C, 39.21; H, 3.52; N, 1.58%. Found: C, 39.06; H, 3.80; N, 1.42%. ^{1}H NMR ($CDCl_3$, 400.13 MHz): δ 0.2–0.4 (m, 6H, 2 × CH_3), 1.0 (dd, 2H, 2 × CH, J = 7; 11 Hz), 1.4 (t, 6H, 2CH_3, J = 7 Hz), 1.9–2.2 (m, 6H, 2 × CH_3), 3.3 (sextet, 2H, 2 × CH, J = 7; 11 Hz), 7.0–8.0 (m, 40H, aromatic). $^{31}P\{^1H\}$ NMR ($CDCl_3$, 161.97 MHz): δ 95.3 (d, J = 69 Hz). UV/Vis: λ_{max} = 313 nm, ε = 22 206 M^{-1} cm^{-1}.

Author contributions

Hendrik G. Visser conceptualized the idea and led the research. R. E. Kroon performed the solid-state PL analyses and did the associated analyses and writing. L. V. Moskaleva led the DFT study, performed the TD-DFT calculations and did the associated writing. M. Schutte-Smith is a co-supervisor of the students involved and did the editing of the final manuscript. D. V. Kama is a co-supervisor and helped with synthesis and writing. K. P. Otukile assisted with running DFT calculations on the CHPC cluster. C. van Staden did all the syntheses and DFT calculations of ground-state geometries as part of his PhD study and wrote the first draft of the paper. C. Matthews contributed to the DFT study and manuscript writing.

Conflicts of interest

There are no conflicts to declare.

Abbreviations

The following abbreviations are used in different contexts to refer to the *N*-substituent/R group on the PNP ligand or in the bis(μ$_2$-bis(diphenylphosphino)-R-amine)-di-gold(I) complex:

2,6Me	2,6-Dimethylphenyl
DIMP	1,2-Dimethylpropyl
*n*Butyl	*n*Bu
*n*Bu	*n*-Butyl
2-Butyl	2-Butyl
*c*Hexyl	Cyclohexyl
*c*Butyl	Cyclobutyl
*c*Pentyl	Cyclopentyl

Data availability

The data sets supporting this article have been uploaded as part of the supplementary information. Supplementary information is available. See DOI: https://doi.org/10.1039/d5dt02181b.

Crystallographic data for (**4b**), (**2b**), (**5b**) and (**1b**) were uploaded to the CCDC. The associated numbers are 2091263 (**4b**), 2091265 (**2b**), 2091267 (**5b**) and 2096913 (**1b**).[72a–d]

Acknowledgements

This work is based on the research supported in part by the National Research Foundation of South Africa (R. E. Kroon, Grant Number 93214, M. Schutte-Smith, Grant Number 116246, C. van Staden, Grant Number 116850, L. Moskaleva, Grant Number 148775). The authors acknowledge the University of the Free State High Performance Computing (HPC) Unit and the Centre for High Performance Computing (CHPC), South Africa, for providing computational resources to this research project. We thank the anonymous reviewers for their valuable comments, which helped improve the clarity of the manuscript and, in particular, for their assistance with the crystallographic refinements.

References

1 A. Deak, C. Jobbagy, A. Demeter, L. Celko, J. Cihlar, P. T. Szabo, P. Abranyi-Balogh, D. E. Crawford, D. Virieux and E. Colacino, Mechanochemical synthesis of mononuclear gold(I) halide complexes of diphosphine ligands with tuneable luminescent properties, *Dalton Trans.*, 2021, **50**, 13337–13344.

2 N. Biricik, Z. Fei, R. Scopelliti and P. J. Dyson, Isolation of an intermediate during the decomposition of a tetragold-phosphane complex, *Eur. J. Inorg. Chem.*, 2004, **2004**, 4232–4236.
3 V. W. Yam and S. W. Choi, Synthesis, photophysics and photochemistry of alkynylgold(I) phosphine complexes, *J. Chem. Soc., Dalton Trans.*, 1996, **6**, 4227–4232.
4 J. M. Forward, D. Bohmann, J. P. Fackler and R. J. Staples, Luminescence studies of gold(I) thiolate complexes, *Inorg. Chem.*, 1995, **34**, 6330–6336.
5 J. M. Forward, Z. Assefa and J. P. Fackler Jr., Photoluminescence of gold(I) phosphine complexes in aqueous solution, *J. Am. Chem. Soc.*, 1995, **117**, 9103–9104.
6 D. Di, A. Romanov, L. Yang, S. Jones, R. Friend, M. Linnolahti and D. Credgington, Highly efficient light-emitting diodes based on intramolecular rotation, *Science*, 2017, **356**, 159–163.
7 Y. Chao, K. Cheng, C. Lin, Y. Chang, Y. Ko, T. Hou and C. Lin, Non-toxic gold nanoclusters for solution-processed white light-emitting diodes, *Sci. Rep.*, 2018, **8**, 8860.
8 C. Wang and C. Yu, Detection of chemical pollutants in water using gold nanoparticles as sensors: a review, *Rev. Anal. Chem.*, 2013, **32**, 1–14.
9 P. Upadhyay, S. Marpu, E. Benton, C. Williams, A. Telang and M. A. Omary, Phosphorescent trinuclear gold(I) pyrazolate chemosensor for silver ion detection and remediation in aqueous media, *Anal. Chem.*, 2018, **90**, 4999–5006.
10 F. Scherbaum, A. Grohmann, G. Müller and H. Schmidbaur, Synthesis, Structure, and Bonding of the Cation $[\{(C_6H_5)_3PAu\}_5C]$, *Angew. Chem., Int. Ed. Engl.*, 1989, **28**, 463–465.
11 H. Schmidbaur, The fascinating implications of new results in gold chemistry, *Gold Bull.*, 1990, **23**, 11–21.
12 P. Pyykko and F. Mendizabal, Theory of the d^{10}–d^{10} closed-shell attraction: 2. Long-distance behaviour and nonadditive effects in dimers and trimers of type $[(X\text{-}Au\text{-}L)_n]$ (n = 2, 3; X = Cl, I, H; L = PH_3, PMe_3, –N≡CH), *Chem. – Eur. J.*, 1997, **3**, 1458–1465.
13 P. Pyykko, Strong closed-shell interactions in inorganic chemistry, *Chem. Rev.*, 1997, **97**, 597–636.
14 N. Runeberg, M. Schutz and H. J. Werner, The aurophilic attraction as interpreted by local correlation methods, *J. Chem. Phys.*, 1999, **110**, 4412–4456.
15 P. Pyykko, Theoretical chemistry of gold, *Angew. Chem., Int. Ed.*, 2004, **43**, 4412–4456.
16 X. Li and J. Cai, Electron density properties and metallophilic interactions of gold halides AuX_2 and Au_2X (X = F–I): Ab initio calculations, *Int. J. Quantum Chem.*, 2016, **116**, 1350–1357.
17 H. Schmidbaur and A. A. Schier, briefing on aurophilicity, *Chem. Soc. Rev.*, 2008, **37**, 1931–1951.
18 H. X. Zhang and C. M. Che, Aurophilic attraction and luminescence of binuclear gold(I) complexes with bridging phosphine ligands: ab initio study, *Chem. – Eur. J.*, 2001, **7**, 4887–4893.
19 G. S. M. Tong, S. C. F. Kui, H. Y. Chao and N. Zhu, The $^3[nd\sigma^*(n+1)p\sigma]$ emissions of linear silver(I) and gold(I) chains with bridging phosphine ligands, *Chem. – Eur. J.*, 2009, **15**, 10777–10789.
20 G. Cui, X. Y. Cao, W. H. Fang, M. Dolg and W. Thiel, Photoinduced gold(I)–gold(I) chemical bonding in dicyanoaurate oligomers, *Angew. Chem., Int. Ed.*, 2013, **52**, 10281–10285.
21 M. Baron, C. Tubaro, A. Biffis, M. Basato, C. Graiff, A. Poater, L. Cavallo, N. Armaroli and G. Accorsi, Blue-emitting dinuclear N-heterocyclic dicarbene gold(I) complex featuring a nearly unit quantum yield, *Inorg. Chem.*, 2012, **51**, 1778–1784.
22 C. Latouche, Y. C. Lee, J. H. Liao, E. Furet, J. Y. Saillard, C. W. Liu and A. Boucekkine, Structure and spectroscopic properties of gold(I) diselenophosph(in)ate complexes: a joint experimental and theoretical study, *Inorg. Chem.*, 2012, **51**, 11851–11859.
23 C. Latouche, Y. R. Lin, Y. Tobon, E. Furet, J. Y. Sailard, C. W. Liu and A. Boucekkine, Au–Au chemical bonding induced by UV irradiation of dinuclear gold(I) complexes: a computational study with experimental evidence, *Phys. Chem. Chem. Phys.*, 2014, **16**, 25840–25845.
24 C. Zeman, Y. H. Shen, J. Heller, K. A. Abboud, K. Schanze and A. Veige, Excited state turn-on of aurophilicity and tunability of relativistic effects in a series of digold triazolates synthesized via iClick, *J. Am. Chem. Soc.*, 2020, **142**, 1–13.
25 F. Groenewald, H. G. Raubenheimer, J. Dillen and C. Esterhuysen, Computational investigation of Au·H hydrogen bonds involving neutral Au^I N-heterocyclic carbene complexes and amphiprotic binary hydrides, *J. Mol. Model.*, 2019, **25**, 135.
26 F. Groenewald, J. Dillen and C. Esterhuysen, Ligand-driven formation of halogen bonds involving Au(I) complexes, *New J. Chem.*, 2018, **42**, 10529–10538.
27 S. De Kock, J. Dillen and C. Esterhuysen, Steric and electronic effects in gold N-heterocyclic carbene complexes revealed by computational analysis, *ChemistryOpen*, 2019, **8**, 539–550.
28 N. Coker, J. A. Bauer and R. Elder, Emission energy correlates with inverse of gold-gold distance for various $[Au(SCN)_2]^-$ salts, *J. Am. Chem. Soc.*, 2004, **126**, 12–13.
29 M. Rawashdeh-Omary, M. Omary, H. Patterson and J. Fackler Jr., Excited-state interactions for $[Au(CN)^{2-}]_n$ and $[Ag(CN)^{2-}]_n$ oligomers in solution. Formation of luminescent gold-gold bonded excimers and exciplexes, *J. Am. Chem. Soc.*, 2001, **123**, 11237–11247.
30 I. Strelnik, V. Gurzhiy, V. Sizov, E. Musina, A. Karasik, S. Tunik and E. Grachova, A stimuli-responsive Au(I) complex based on an aminomethylphosphine template: synthesis, crystalline phases and luminescence properties, *CrystEngComm*, 2016, **18**, 7629–7635.
31 H. Schmidbaur and H. Raubenheimer, Excimer and exciplex formation in gold(I) complexes preconditioned by aurophilic interactions, *Angew. Chem., Int. Ed.*, 2020, **59**, 14748–14771.

32 W. Duminy, M. N. Pillay and W. E. van Zyl, Silver(I) and gold(I) monothiocarbonate complexes: synthesis, structure, luminescence, *Inorganics*, 2022, **10**, 19.

33 W. F. Fu, K. C. Chan, V. M. Miskowski and C. M. Che, The Intrinsic ^{3}[dσ*pσ] emission of binuclear gold(I) complexes with two bridging diphosphane ligands lies in the near UV; emissions in the visible region are due to exciplexes, *Angew. Chem., Int. Ed.*, 1999, **38**, 2783–2785.

34 K. H. Leung, D. L. Phillips, M. C. Tse and V. M. Miskowski, Resonance Raman investigation of the Au(I)–Au(I) interaction of the ^{1}[dσ*pσ] excited state of $Au_2(dcpm)_2(ClO_4)_2$ (dcpm = Bis(dicyclohexylphosphine)methane), *J. Am. Chem. Soc.*, 1999, **121**, 4799–4803.

35 W. F. Fu, K. C. Chan, K. K. Cheung and C. M. Che, Substrate-binding reactions of the ^{3}[dσ*pσ] excited state of binuclear gold(I) complexes with bridging bis(dicyclohexylphosphino)methane ligands: emission and time-resolved absorption spectroscopic studies, *Chem. – Eur. J.*, 2001, **7**, 4656–4664.

36 T. Penfold, S. Karlson, G. Capano, F. Lima, J. Rittmann, M. Reinhard and M. Chergui, Solvent-induced luminescence quenching: static and time-resolved X-ray absorption spectroscopy of a copper(I) phenanthroline complex, *J. Phys. Chem.*, 2013, **117**, 4591–4601.

37 A. Assefa, B. G. McBurnett, R. J. Staples and J. P. Fackler, Structures and spectroscopic properties of gold(I) complexes of 1,3,5-Triaza-7-phosphaadamantane (TPA). 2. Multiple-state emission from (TPA)AuX (X = Cl, Br, I) complexes, *Inorg. Chem.*, 1995, **20**, 4965–4972.

38 W. E. van Zyl, J. M. López-de-Luzuriaga, A. A. Mohamed, R. J. Staples and J. P. Fackler Jr., Dinuclear gold(I) dithiophosphonate complexes: synthesis, luminescent properties, and X-ray crystal structures of $[AuS_2PR(OR')]_2$ (R = Ph, R′ = C_5H_9; R = 4-C_6H_4OMe, R′ = (1S,5R,2S)-(−)-menthyl; R = Fc, R′ = $(CH_2)_2O(CH_2)_2$OMe), *Inorg. Chem.*, 2002, **41**, 4579–4589.

39 R. L. White-Morris, M. M. Olmstead, A. L. Balch, O. Elbjeirami and M. A. Omary, Orange luminescence and structural properties of three isostructural halocyclohexylisonitrilegold(I) complexes, *Inorg. Chem.*, 2003, **42**, 6741–6748.

40 W.-F. Fu, K.-C. Chan, V. M. Miskowski and C.-M. Che, The Intrinsic ^{3}[dσ*pσ] Emission of Binuclear Gold(I) Complexes with Two Bridging Diphosphane Ligands Lies in the Near UV; Emissions in the Visible Region Are Due to Exciplexes, *Angew. Chem., Int. Ed.*, 1999, **38**, 2783–2785.

41 M. Saitoh, A. L. Balch, J. Yuasa and T. Kawai, Effects of Counter Anions on Intense Photoluminescence of 1-D Chain Gold(I) Complexes, *Inorg. Chem.*, 2010, **49**, 7129–7134.

42 L. M. C. Luong, M. A. Malwitz, V. Moshayedi, M. M. Olmstead and A. L. Balch, Role of Anions and Mixtures of Anions on the Thermochromism, Vapochromism, and Polymorph Formation of Luminescent Crystals of a Single Cation, $[(C_6H_{11}NC)_2Au]$, *J. Am. Chem. Soc.*, 2020, **142**, 5689–5701.

43 N. Kathewad, N. Kumar, R. Dasgupta, M. Ghosh, S. Pal and S. Khan, The syntheses and photophysical properties of PNP-based Au(I) complexes with strong intramolecular Au···Au interactions, *Dalton Trans.*, 2019, **48**, 7274–7280.

44 S. Pal, N. Kathewad, R. Pant and S. Khan, Synthesis, characterization, and luminescence studies of gold(I) complexes with PNP- and PNB-Based ligand systems, *Inorg. Chem.*, 2015, **54**, 10172–10183.

45 A. V. Paderina, I. O. Koshevoy and E. V. Gracheva, Keep it tight: a crucial role of bridging phosphine ligands in the design and optical properties of multinuclear coinage metal complexes, *Dalton Trans.*, 2021, **50**, 6003.

46 H. G. Raubenheimer and H. Schmidbaur, The late start and amazing upswing in gold chemistry, *J. Chem. Educ.*, 2014, **91**, 2024–2036.

47 J. R. Shakirova, E. V. Grachova, V. V. Gurzhiy, I. O. Koshevoy, A. S. Melnikov, O. V. Sizova, S. P. Tunik and A. Laguna, Luminescent heterometallic gold–copper alkynyl complexes stabilized by tridentate phosphine, *Dalton Trans.*, 2012, **41**, 2941–2949.

48 F. Krätschmer, X. Gui, M. T. Gamer, W. Klopper and P. W. Roesky, Systematic investigation of the influence of electronic substituents on dinuclear gold(I) amidinates: synthesis, characterisation and photoluminescence studies, *Dalton Trans.*, 2022, **51**, 5471.

49 C. King, J. C. Wang, M. N. I. Khan and J. P. Fackler Jr., Luminescence and metal-metal interactions in binuclear gold(I) compounds, *Inorg. Chem.*, 1989, **28**, 2145–2149.

50 Q. J. Pan and H. X. Zhang, An ab initio study on luminescent properties and aurophilic attraction of binuclear gold (I) complexes with phosphinothioether ligands, *Inorg. Chem.*, 2004, **43**, 593–601.

51 M. Baroncini, G. Bergamini and P. Ceroni, Rigidification or interaction-induced phosphorescence of organic molecules, *Chem. Commun.*, 2017, **53**, 2081–2093.

52 A. Becke, Density–functional thermochemistry. III. The role of exact exchange, *J. Chem. Phys.*, 1993, **98**, 5648–5652.

53 C. Lee, W. Yang and R. Parr, Development of the Colle-Salvetti correlation-energy formula into a functional of the electron density, *Phys. Rev. B: Condens. Matter Mater. Phys.*, 1988, **37**, 785–789.

54 P. Stephens, F. Devlin, C. Chabalowski and M. Frisch, Ab initio calculation of vibrational absorption and circular dichroism spectra using density functional force fields, *J. Phys. Chem.*, 1994, **98**, 11623–11627.

55 V. Staroverov, G. Scuseria, J. Tao and J. Perdew, Comparative assessment of a new nonempirical density functional: molecules and hydrogen-bonded complexes, *J. Chem. Phys.*, 2003, **119**, 12–129.

56 F. Weigend and R. Ahlrichs, Balanced basis sets of split valence, triple zeta valence and quadruple zeta valence quality for H to Rn: Design and assessment of accuracy, *Phys. Chem. Chem. Phys.*, 2005, **7**, 3297–3305.

57 F. Weigend, Accurate Coulomb-fitting basis sets for H to Rn, *Phys. Chem. Chem. Phys.*, 2006, **8**, 1057–1065.

58 S. Grimme, J. Antony, S. Ehrlich and H. Krieg, A consistent and accurate ab initio parametrization of density func-

tional dispersion correction (DFT-D) for the 94 elements H-Pu, *J. Chem. Phys.*, 2010, **132**, 154104.
59 S. Grimme, S. Ehrlich and L. Goerigk, Effect of the damping function in dispersion corrected density functional theory, *J. Comput. Chem.*, 2011, **32**, 1456–1465.
60 M. J. Frisch, G. W. Trucks, H. B. Schlegel, G. E. Scuseria, M. A. Robb, J. R. Cheeseman, G. Scalmani, V. Barone, G. A. Petersson, H. Nakatsuji, X. Li, M. Caricato, A. V. Marenich, J. Bloino, B. G. Janesko, R. Gomperts, B. Mennucci, H. P. Hratchian, J. V. Ortiz, A. F. Izmaylov, J. L. Sonnenberg, D. Williams-Young, F. Ding, F. Lipparini, F. Egidi, J. Goings, B. Peng, A. Petrone, T. Henderson, D. Ranasinghe, V. G. Zakrzewski, J. Gao, N. Rega, G. Zheng, W. Liang, M. Hada, M. Ehara, K. Toyota, R. Fukuda, J. Hasegawa, M. Ishida, T. Nakajima, Y. Honda, O. Kitao, H. Nakai, T. Vreven, K. Throssell, J. A. Montgomery Jr., J. E. Peralta, F. Ogliaro, M. J. Bearpark, J. J. Heyd, E. N. Brothers, K. N. Kudin, V. N. Staroverov, T. A. Keith, R. Kobayashi, J. Normand, K. Raghavachari, A. P. Rendell, J. C. Burant, S. S. Iyengar, J. Tomasi, M. Cossi, J. M. Millam, M. Klene, C. Adamo, R. Cammi, J. W. Ochterski, R. L. Martin, K. Morokuma, O. Farkas, J. B. Foresman and D. J. Fox, *Gaussian 16, Revision C.01*, Gaussian, Inc., Wallingford CT, 2016.
61 R. D. Dennington, T. A. Keith, and J. M. Millam, *GaussView, Version 5.0.9*, Semichem Inc., Shawnee Mission, KS, 2008.
62 P. Ros and G. C. A. Schuit, Molecular orbital calculations on copper chloride complexes, *Theor. Chim. Acta*, 1966, **4**, 1–12.
63 T. Lu and F. Chen, Multiwfn: a multifunctional wavefunction analyzer, *J. Comput. Chem.*, 2012, **33**, 580–592.
64 Bruker AXS Inc. Bruker, *APEX3 Crystallography Software Suite*. 2016.
65 Bruker AXS Inc. Bruker, *SAINT*, Crystallography Software Suite. 2016.
66 G. M. Sheldrick, SHELXT – Integrated space-group and crystal-structure determination, *Acta Crystallogr., Sect. A: Found. Adv.*, 2015, **71**, 3–8.
67 G. M. Sheldrick, A short history of SHELX, *Acta Crystallogr., Sect. A: Found. Crystallogr.*, 2008, **64**, 112–122.
68 O. V. Dolomanov, L. J. Bourhis, R. J. Gildea, J. A. K. Howard and H. J. Puschmann, OLEX2: A complete structure solution, refinement and analysis program, *Appl. Crystallogr.*, 2009, **42**, 339–341.
69 L. J. Farrugia, WinGX and ORTEP for Windows: An update, *J. Appl. Crystallogr.*, 2012, **45**, 849–854.
70 H. Putz and K. Brandenburg, *Diamond crystal and molecular structure visualization*, Crystal Impact, 2023.
71 W. Armarego and C. Chai, *Purification of laboratory chemicals*, Butterworth Heinemann, Burlington, 5th edn, 2003.
72 (*a*) CCDC 2091263: Experimental Crystal Structure Determination, 2025, DOI: 10.5517/ccdc.csd.cc28643r; (*b*) CCDC 2091265: Experimental Crystal Structure Determination, 2025, DOI: 10.5517/ccdc.csd.cc28645t; (*c*) CCDC 2091267: Experimental Crystal Structure Determination, 2025, DOI: 10.5517/ccdc.csd.cc28647w; (*d*) CCDC 2096913: Experimental Crystal Structure Determination, 2025, DOI: 10.5517/ccdc.csd.cc28d0c2.